

Global Biogeochemical Cycles®










RESEARCH ARTICLE

10.1029/2020GB006851

Simulated Future Trends in Marine Nitrogen Fixation Are Sensitive to Model Iron Implementation

Key Points:

- Models performing similarly with respect to global NO₃, PO₄, and O₂ distributions yield diverse responses in marine N₂ fixation to warming
- Marine N₂ fixation trends are sensitive to whether iron limits primary production in upwelling regions, for example, the Eastern Tropical Pacific

Wanxuan Yao¹ , Karin F. Kvale^{1,2} , Wolfgang Koeve¹ , Angela Landolfi³ ,
Eric Achterberg¹ , Erin M. Bertrand⁴ , and Andreas Oschlies¹ 

¹GEOMAR Helmholtz Centre for Ocean Research Kiel, Kiel, Germany, ²Now at GNS Science, Lower Hutt, New Zealand, ³ISMAR, National Research Council, Rome, Italy, ⁴Department of Biology, Dalhousie University, Halifax, NS, Canada

Correspondence to:

W. Yao,
wyao@geomar.de

Citation:

Yao, W., Kvale, K. F., Koeve, W., Landolfi, A., Achterberg, E., Bertrand, E. M., & Oschlies, A. (2022). Simulated future trends in marine nitrogen fixation are sensitive to model iron implementation. *Global Biogeochemical Cycles*, 36, e2020GB006851. <https://doi.org/10.1029/2020GB006851>

Received 3 OCT 2020
Accepted 7 FEB 2022

Abstract Biological nitrogen fixation is an important oceanic nitrogen source, potentially stabilizing marine fertility in an increasingly stratified and nutrient-depleted ocean. Iron limitation of low latitude primary producers has been previously demonstrated to affect simulated regional ecosystem responses to climate warming or nitrogen cycle perturbation. Here we use three biogeochemical models that vary in their representation of the iron cycle to estimate change in the marine nitrogen cycle under a high CO₂ emissions future scenario (RCP8.5). The first model neglects explicit iron effects on biology (NoFe), the second utilizes prescribed, seasonally cyclic iron concentrations and associated limitation factors (FeMask), and the third contains a fully dynamic iron cycle (FeDyn). Models were calibrated using observed fields to produce near-equivalent nutrient and oxygen fits, with productivity ranging from 49 to 75 Pg C yr⁻¹. Global marine nitrogen fixation increases by 71.1% with respect to the preindustrial value by the year 2100 in NoFe, while it remains stable (0.7% decrease in FeMask and 0.3% increase in FeDyn) in explicit iron models. The mitigation of global nitrogen fixation trend in the models that include a representation of iron originates in the Eastern boundary upwelling zones, where the bottom-up control of iron limitation reduces export production with warming, which shrinks the oxygen deficient volume, and reduces denitrification. Warming-induced trends in the oxygen deficient volume in the upwelling zones have a cascading effect on the global nitrogen cycle, just as they have previously been shown to affect tropical net primary production.

Plain Language Summary Phytoplankton need nutrients to grow. Two of those nutrients are nitrogen and iron. Climate change projections suggest that in the future there could be less nitrogen supplied to the surface ocean, which might reduce phytoplankton growth. Less phytoplankton growth could impact a wide range of ocean services, like fishing and fossil carbon draw-down. However, some phytoplankton have the ability to add “new” nitrogen to the surface ocean directly from the atmosphere. In this study, we explore how this biological fixation of new nitrogen might change into the future using three models. These models differ in how iron is represented, but all do equally well in representing the observed nutrient and oxygen distribution. Biological nitrogen fixation slightly decreases with climate change in the very complex iron model and the moderately complex iron model, but it increases strongly (by more than 70% by the year 2100) in the model that does not include iron effects on biology. Our study addresses the importance of iron models and how they can change our view of how the ocean responds to climate change.

1. Introduction

Marine ecosystems provide crucial services to humanity, yet are under pressure due to climate change. Most global earth system models agree on a future ocean with increasing stratification and decreasing nutrient re-supply to the surface mixed layer, particularly in low and mid-latitudes (Cabr e et al., 2015). How marine ecosystems will respond to these changing conditions is uncertain. The growth of phytoplankton is controlled by nutrient and light limitation, temperature, and grazing pressure (Parsons et al., 1984). Differences in model parameterization can lead to wide-ranging ecosystem responses to transient forcing (e.g., Kwiatkowski et al., 2014; Taucher & Oschlies, 2011). Climate model intercomparison reveals that while ocean surface temperature, pH and global oxygen (O₂) content show relatively similar trends across models, the change in simulated global net primary production (NPP) by the end of the 21st century varies widely both in magnitude and sign, with particularly large differences in low latitude NPP trends (Bopp et al., 2013). This spread in model projections of NPP is attributed to differences in parameterization of surface nutrient re-supply pathways, for example, including vertical mixing,

© 2022. The Authors.

This is an open access article under the terms of the [Creative Commons Attribution License](https://creativecommons.org/licenses/by/4.0/), which permits use, distribution and reproduction in any medium, provided the original work is properly cited.

the remineralization of organic particles, zooplankton grazing and microbial loop recycling, in addition to the strength of nutrient limitation realized in the different models (Landolfi et al., 2017; Laufkötter et al., 2015).

Nitrogen (N) is an important nutrient in the marine ecosystem. In an increasingly nutrient-limited surface ocean, processes that could add “new” N are potentially important for the maintenance of ocean fertility. The biological fixation of dinitrogen (N_2) by diazotrophs is a major natural source of fixed N to the ocean (100–200 TgNyr⁻¹, Gruber & Galloway, 2008; Karl et al., 2002). Newly fixed N becomes biologically available to non-diazotrophic phytoplankton (Mulholland, 2007). Earth system models produce a range of N_2 fixation trends under climate change, which arise from differences in model structure (Wrightson & Tagliabue, 2020).

Improving the constraints on future N_2 fixation trends requires an improved understanding of the processes critical for modern ocean N_2 fixation. Spatial patterns of N_2 fixation are thought to be determined by temperature (Breitbarth et al., 2007; F. Fu et al., 2014), availability of micro and macro nutrients, and grazing pressure. All three drivers are susceptible to warming effects from climate change (Laufkötter et al., 2015). Due to their effects on the macro-nutrient ratio, denitrification and anammox are considered key processes modulating the activity of diazotrophs. Denitrification and anammox that occur in low oxygen environments (such as in tropical upwelling zones) change the relative availability of nitrate (NO_3) and phosphate (PO_4) in the surface ocean downstream (Deutsch et al., 2007; Weber & Deutsch, 2014). The resulting stoichiometrically excess phosphate (positive P^* , defined as $PO_4 - NO_3/16$, Deutsch et al., 2007) might provide diazotrophs with a competitive advantage relative to other types of phytoplankton. This competitive advantage is hypothesized to explain why rates of N_2 fixation are enhanced in the NO_3 -depleted low latitude surface ocean (Deutsch et al., 2007; N. S. Garcia et al., 2015; Tyrrell, 1999).

At the same time, iron (Fe) is essential for all phytoplankton as it is needed to form a range of cellular enzymes that are associated with photosynthesis and respiration. However, diazotrophs additionally require iron for producing the N_2 fixation enzyme nitrogenase (Kustka et al., 2003; Raven, 1988; Tagliabue et al., 2017; Zehr & Capone, 2020), causing diazotroph growth to be particularly sensitive to a lack of iron. For diazotrophs, the supply of iron is so essential that its availability helps to define the biogeography of N_2 fixation (Bonnet et al., 2017; Knapp et al., 2016; C. M. Moore et al., 2009; Schlosser et al., 2014; Ward et al., 2013). Unfortunately, global ocean models still have a hard time reproducing the observed iron concentrations (Tagliabue et al., 2016) and simulated patterns of N_2 fixation also have large uncertainties (Landolfi et al., 2018).

Iron availability is expected to affect denitrification patterns in the ocean (Landolfi et al., 2013). Biological productivity is limited by iron availability over one-third of the surface ocean, including the Eastern Tropical Pacific (ETP) upwelling zones (C. M. Moore et al., 2013). This limitation can impact particulate organic matter export (Martin, 1990). Therefore, a change in iron availability in a highly productive upwelling zone might alter particulate organic matter export and thereby influence the extent and intensity of oxygen deficient zones (ODZs) and of denitrification. In their modeling study, Buchanan et al. (2019) showed that an increase in iron availability in the ETP can lead to a larger ODZ, and a downstream enhancement of diazotroph biomass and N_2 fixation. They inferred that this process could have contributed an additional 7–16 ppm of carbon dioxide (CO_2) sequestration in the tropical ocean in the Last Glacial Maximum (Buchanan et al., 2019).

In addition to bottom-up controls via iron availability and denitrification, top-down control of diazotrophy by zooplankton grazing might also influence the global patterns of N_2 fixation (Landolfi et al., 2021; Wang et al., 2019). Landolfi et al. (2021) present a top-down control framework which explains the maintenance of a niche for diazotrophs in nutrient-rich environments by selective grazing pressure on non nitrogen-fixing phytoplankton.

Here we examine what controls the global N_2 fixation response to global warming in three marine biogeochemical models with different representations of the marine iron cycle, all of which perform similarly with respect to reproducing observed NO_3 , PO_4 , and O_2 distribution (Yao et al., 2019). All three models were individually subjected to parameter optimization and their preindustrial steady-states were assessed in Yao et al. (2019). Our objective is not to simply assess the role of iron limitation, as has been done previously, for example, J. K. Moore and Doney (2007), but to examine how differences in nutrient cycling impact transient model behavior. We first describe the models and the new transient global-warming experiments. Then, we compare the different simulated responses of N_2 fixation to global warming. Next, we examine the impact of ODZ development

and denitrification on N_2 fixation. We link the development of ODZs to in situ export production trends via the different assumptions about nutrient pathways in the different models, and make some recommendations for further model improvements.

2. Methods

2.1. Model Description

In this study, we use the University of Victoria Earth System Climate Model (UVicESCM, version 2.9; Eby et al., 2013; Weaver et al., 2001). The UVicESCM is an earth system model of intermediate complexity. It contains four components: a simple one-layer atmospheric model, a terrestrial model (Meissner et al., 2003), a sea-ice model and a three-dimensional ocean general circulation model. All components have a horizontal grid resolution of 3.6° in meridional and 1.8° in zonal direction. The one-layer atmospheric model is based on an energy-moisture balance scheme (assuming lateral heat and moisture transport by diffusion; Fanning & Weaver, 1996), which calculates heat and water fluxes between the atmosphere and the ocean, land and sea ice dynamically, while applying prescribed (NCAR/NCEP) winds. A thermodynamic sea-ice model (Bitz & Lipscomb, 1999) is used, while constant continental ice sheets are prescribed. The ocean component is the Modular Ocean Model 2 (MOM2). It has 19 vertical layers with increasing thickness from 50 m at the surface to 500 m in the deep ocean. The ocean advection scheme is a non-linear second-order Flux-Corrected Transport scheme (Weaver & Eby, 1997).

2.2. Biogeochemical Models and Parameterization

We apply three variants of the marine biogeochemical component in the UVicESCM, which differ in their treatment of the iron cycle. All of them are nutrient-phytoplankton-zooplankton-detritus (NPZD) models with two types of phytoplankton, ordinary phytoplankton and diazotrophs, one zooplankton, and detritus. In the models, the growth of phytoplankton is governed by nutrients, light and temperature. In all three models, diazotrophs grow slower than ordinary phytoplankton but can also fix N_2 to meet their N demand when NO_3 is limiting (equations are given in appendix).

The first model contains no representation of the iron cycle (NoFe, created by disabling iron limitation in the model presented by Keller et al. [2012]). The second model variant is that of Keller et al. (2012) and makes use of a prescribed, seasonally periodic iron concentration mask (FeMask; Keller et al., 2012), by regridding the output of the Biology Light Iron Nutrient and Gases model (BLING; Galbraith et al., 2010). The third variant includes a fully dynamic iron cycle (FeDyn; Nickelsen et al., 2015), which resolves major sources and sinks of iron in the ocean, for example, dust deposition, benthic release, particle scavenging, colloid formation, remineralization as well as hydrothermal release (Yao et al., 2019). In the models that include iron (FeMask and FeDyn), both diazotroph and ordinary phytoplankton growth rates are reduced when iron is limiting, in addition to the usual controlling factors, for example, macro-nutrient(s), light and temperature. In the model without iron (NoFe), the growth rates of diazotrophs and ordinary phytoplankton do not depend on the iron concentration. The use of an externally derived iron mask (BLING) in FeMask, rather than one produced by FeDyn was decided for pragmatic reasons. FeMask has been, and continues to be, widely used in the UVicESCM user community for a variety of research questions (Getzlaff & Dietze, 2013; Mengis et al., 2018; Somes & Oschlies, 2015). Therefore it is useful for us to calibrate it, and to assess how its optimal configuration behaves transiently compared to other model versions. However, application of a FeDyn-derived iron mask to the FeMask calibration would also prove redundant, as the model structures are identical with respect to iron uptake by biology. BLING (used in FeMask) and FeDyn has different iron concentrations in the surface due to a lot of different factors, for example, different dust deposition, sediment release, biological uptake, scavenging parameterization, and different physics. This is why iron half saturation parameters for phytoplankton were included in the model calibration by Yao et al. (2019). Details, including equations, of each model configuration can be found in Nickelsen et al. (2015, FeDyn) and Keller et al. (2012, FeMask and NoFe). Note that the objective of our current study is not a comparison of full, partial or absent consideration of the influence of iron limitation in a preindustrial steady state, which has been dealt with by Yao et al. (2019), but instead a comparison of model behavior under transient forcing. These models have different parameterizations resulting from parameter calibration (see details below) against the same set of

observational nutrient and oxygen distributions. These model differences have implications for nitrogen fixation responses to climate warming.

2.3. Model Calibration

The models used in this study have different structures and were hand-tuned to different objectives in prior studies (Keller et al., 2012; Nickelsen et al., 2015). Hence, they have different representations of ocean biogeochemical tracer distributions. In order to perform a “fair” comparison between different models, we first needed to calibrate all models using the same objective against the same set of observational data, which was done in an earlier study by Yao et al. (2019).

In Yao et al. (2019), we first chose a subset of biogeochemical parameters for FeDyn (six out of 44; see Table B1) for its calibration. Those parameters are among the most sensitive and/or most uncertain (few or no measurements available) and at the same time provide a large coverage of control in the different biogeochemical domains, for example, iron, nitrogen, oxygen, phytoplankton and zooplankton biomass. For the calibration of NoFe and FeMask, we chose sets of parameters that are as close to the FeDyn set as possible (see Table B1). We then calibrated all three models against the same global set of observational NO_3 , PO_4 , and O_2 concentrations (World Ocean Atlas 2013; H. E. Garcia et al., 2013a, 2013b) with the help of an evolutionary optimization algorithm, which minimizes the model misfits. After calibration, we found that all models have relatively similar performance reproducing the observed NO_3 , PO_4 , and O_2 distributions (less than 5% difference between rms model-data misfits) in an assumed preindustrial steady-state. Residual model misfits for NO_3 , PO_4 , and O_2 are only about 15% of their observed global mean concentration.

We next assessed each model's synthetic global biogeochemical fluxes and indicators, for example, NPP, export production, flux of organic carbon at a depth of 2 km, denitrification, the volume fraction of the ocean with suboxic conditions (oxygen concentrations less than $5 \text{ mmol O}_2 \text{ m}^{-3}$), and the volume fraction of the ocean with hypoxic conditions (oxygen concentrations less than $50 \text{ mmol O}_2 \text{ m}^{-3}$). We found that in steady-state, all models simulate observed global biogeochemical fluxes and indicators (four out of six) to a similar degree. Although NoFe simulates a 50% higher NPP compared to the model with the lowest estimate (FeMask), the range is $49.1\text{--}74.8 \text{ Pg C yr}^{-1}$ between the three calibrated models. This spread is smaller than the $32\text{--}77 \text{ Pg C yr}^{-1}$ range reported from 24 independent estimates (based either on ocean color observations, on ecosystem models, or on biogeochemical models - a wide range of methodologies) in Carr et al. (2006). Different flux values arise between calibrated models as the model calibrations seek to achieve optimal fit to nutrient distributions using the parameters available in the different models, whose structures vary (presence or absence of iron limitation, namely). For example, in the models which include iron limitation, the calibration exploited this bottom-up control to limit NPP. However, in NoFe the calibration compensated for the absence of iron limitation using top-down control, with a larger resulting grazing parameter value and also greater global NPP rates. It is interesting to note that the wide range of NPP rates achievable with similar model performance with respect to nutrient and oxygen distributions indicates only minor relevance of NPP for general model tuning of these metrics. This is because NPP can be compensated by opposing fluxes in the model. In Yao et al. (2019) the surface total nutrient recycling (sum of the microbial loop recycling, zooplankton excretion and remineralization) compensates the differences of NPP and produces similar export production rates ($6.3\text{--}7.1 \text{ Pg C yr}^{-1}$) out of the euphotic zone (130 m) for all three calibrated models. It also highlights the importance of including additional metrics, as a target for model calibration when attempting to produce a complete picture of ocean biogeochemistry. Another indicator exhibiting variability between the three calibrated models is the volume fraction of the ocean with suboxic conditions. This is not surprising considering the fraction of suboxic water occupies only around 0.2 (World Ocean Atlas 2013; H. E. Garcia et al., 2013b) of the total ocean volume, and our calibrations were focused on the overall NO_3 , PO_4 , and O_2 distributions. More details about our calibration and resulting differences in optimal nutrient pathways for each model can be found in Yao et al. (2019).

2.4. Model Experiments

All models are integrated for 10 thousand years with preindustrial (year 1800) climate boundary conditions to reach equilibrium. A prescribed historical and “business-as-usual” RCP8.5 atmospheric CO_2 concentration

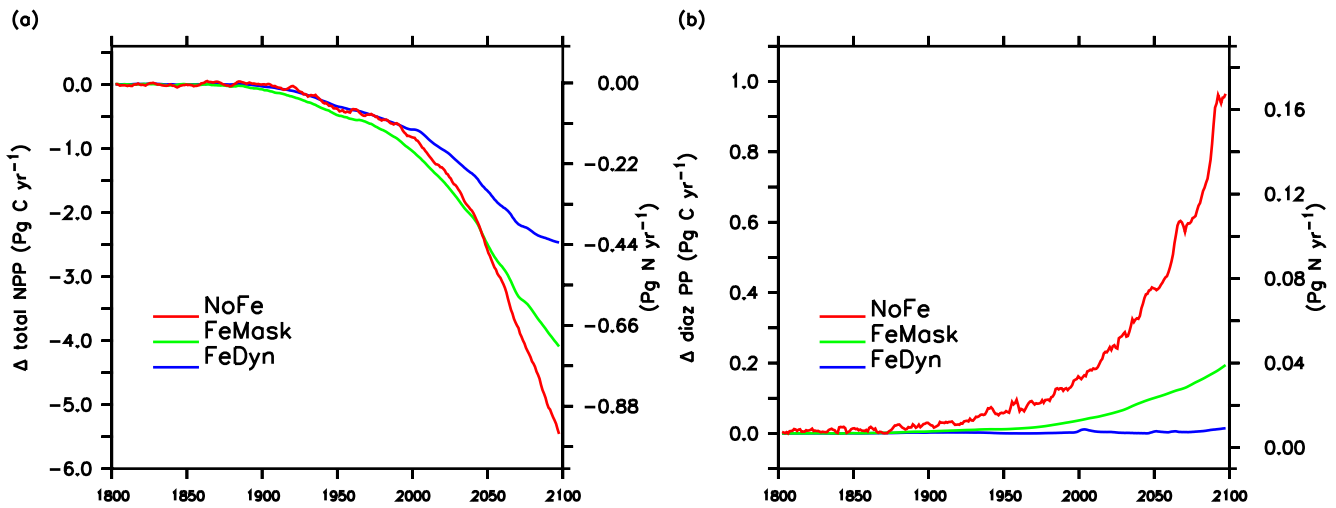


Figure 1. Simulated change in 5-yearly averaged global marine NPP (a) and diazotroph primary production (b) between 1800 and 2100 for all models: NoFe (red), FeMask (green) and FeDyn (blue). The maps of NPP and its change are shown in Figures B1–B3.

forcing (van Vuuren et al., 2011) is then applied from year 1800–2100, but with climatological seasonally cycling NCAR/NCEP wind fields. The preindustrial physical circulation and circulation responses are identical in all three model configurations. Atmospheric iron deposition flux (Luo et al., 2008), which is a preindustrial climatological estimate of monthly iron deposition, is not changed during the transient experiment in FeDyn. We do not include atmospheric N deposition in this study, which was found to be of minor importance in an earlier study by Landolfi et al. (2017).

3. Results and Discussion

3.1. Simulated Trends in Global NPP and Diazotroph Primary Production

Global total primary production in year 1800 is 74.8 (NoFe), 49.4 (FeMask), and 50.4 (FeDyn) Pg C yr⁻¹. In all simulations, NPP decreases with time (Figure 1a), in general agreement with the trends of CMIP5 models (Bopp et al., 2013; Laufkötter et al., 2015). Laufkötter et al. (2015) report a range of 15% to +30% (4.3 to +10 Pg C yr⁻¹) NPP change by year 2100 from baseline values of 17–83 Pg C yr⁻¹ for a 1998–2007 climatology. In the year 2100, the largest absolute decline is found in NoFe (5.6 Pg C yr⁻¹) and the largest percentage decline in FeMask (9.16%). Differences in projected NPP are not due simply to the presence or absence of iron in the models; each model had previously been calibrated against observed biogeochemical tracer distributions in an objective model-tuning exercise to achieve as-similar-as possible model performance against PO₄, NO₃, and O₂. The calibration framework achieved this objective by adjusting biogeochemical parameter values in a way that also produced differences in nutrient pathways and differences in fluxes and biogeochemical rates (Yao et al., 2019). However, despite these remaining differences in fluxes between models, the inter-model NPP spread in our calibrated model suite with identical physics is smaller than that found across CMIP5 models (Yao et al., 2019).

Global diazotroph primary production in year 1800 is 0.6 (NoFe), 0.3 (FeMask), and 0.4 (FeDyn) Pg C yr⁻¹. In contrast to global NPP, diazotroph primary production increases in all simulations (by 0.02–1.0 Pg C yr⁻¹ between 1800 and 2100; Figure 1b). When compared with total NPP, the relative importance of diazotroph primary production to total NPP increases between 1800 and 2100. In 1800, diazotroph primary production contributes 0.76% (NoFe), 0.57% (FeMask), and 0.75% (FeDyn) to global NPP and in 2100 it increases to 2.3% of global NPP in NoFe, 1.1% in FeMask and 0.82% in FeDyn.

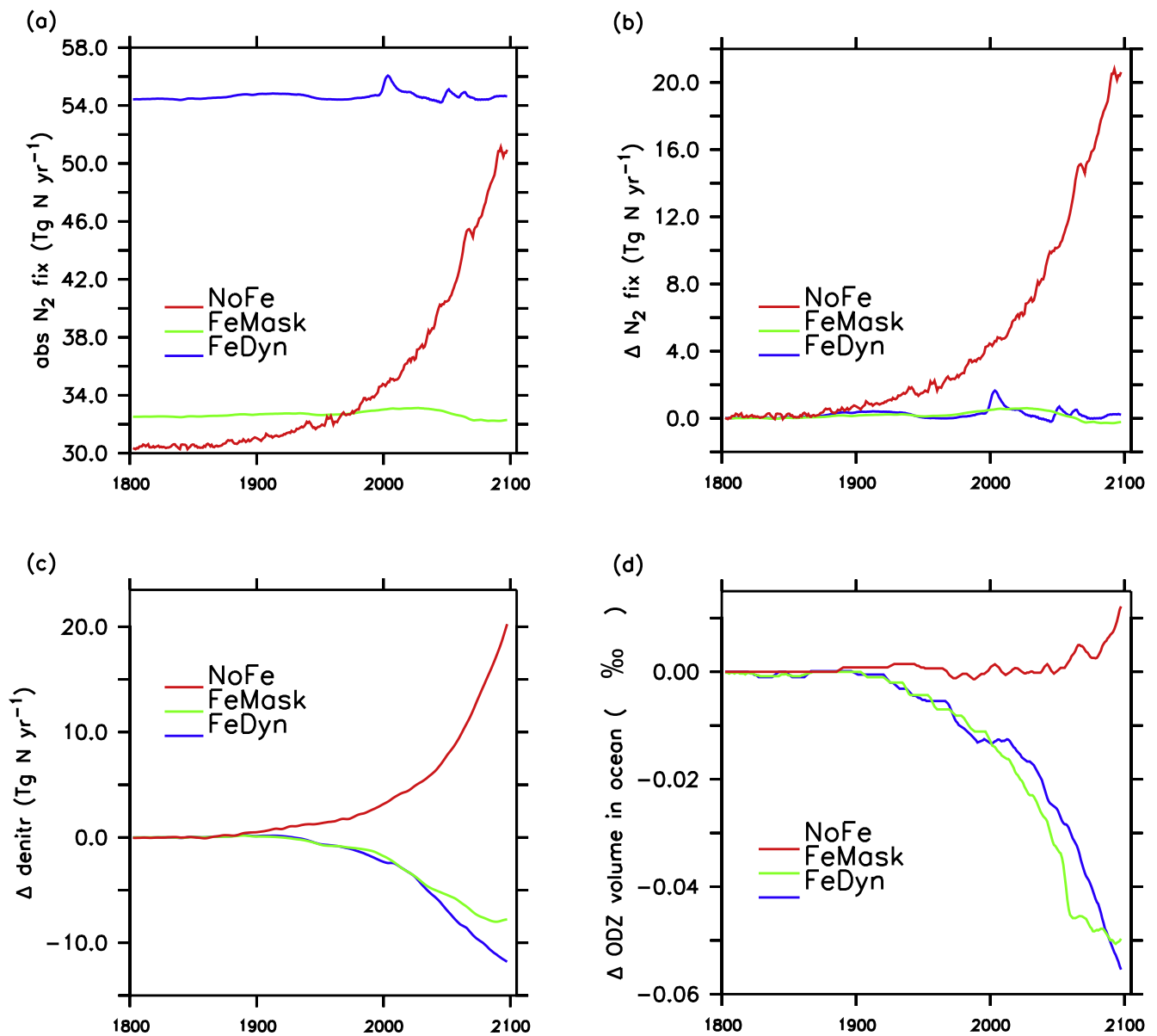


Figure 2. Simulated running 5-year-averaged global N₂ fixation rates (a), their temporal changes (b), temporal changes of denitrification (c) and the changes in ODZ volume (d, change in the percentage of the total ocean volume) between 1800 and 2100. Note: we define ODZ as regions where O₂ concentration is below 5 mmol m⁻³. A global map of N₂ fixation is shown in Figure B4.

3.2. Trends in Simulated N₂ Fixation

Steady-state rates as well as trends in N₂-fixation also show remarkable differences across the model suite. The simulated preindustrial N₂ fixation rates are between 30.3 and 54.1 Tg N yr⁻¹ (Figure 2a). The calibrated NoFe has the smallest preindustrial N₂ fixation rate, which is also much smaller than earlier, hand-tuned versions of the UVicESCM that applied different parameter values and also did not include iron (UVicESCM version 2.7, 316 Tg N yr⁻¹, Riche & Christian, 2018; UVicESCM version 2.8 & 2.9, 150 Tg N yr⁻¹, Keller et al., 2012; Oschlies et al., 2019; UVicESCM version 2.9 with additional structural changes including benthic denitrification, 110–126 Tg N yr⁻¹, Landolfi et al., 2017). This low N₂ fixation value occurs in NoFe because of the relatively efficient near-surface nutrient recycling in this model, which minimizes denitrification and therefore N₂ fixation in the preindustrial steady-state configuration (Yao et al., 2019). Applying a dynamic iron cycle (FeDyn) in the model results, after calibration, in an optimal parameter set which produces the largest preindustrial N₂ fixation

rate ($54.1 \text{ Tg N yr}^{-1}$) among the three models. However, even the FeDyn N_2 fixation rate is in the lower range of observations and model estimates (between 89 and 213 Tg N yr^{-1} ; Landolfi et al., 2018). Note, that independent estimates of the N_2 fixation rate were not used as an explicit constraint in the calibration of Yao et al. (2019). Furthermore, none of the models include benthic denitrification, which could increase global total denitrification and enhance global N_2 fixation (Weber & Deutsch, 2014).

The simulated evolution of N_2 fixation in response to global warming differs considerably between simulations (Figures 2a and 2b). While N_2 fixation increases by $21.6 \text{ Tg N yr}^{-1}$ (71%) in NoFe between 1800 and 2100, fixation rates remain almost unaffected by global warming in FeMask and FeDyn. Landolfi et al. (2017) reported an increase by 0.3% in N_2 fixation due to the increasing PO_4 limitation for the same simulated period in a version of UVicESCM with prescribed iron concentrations (which includes a representation of nitrous oxide and has a different set of parameter values comparing to FeMask). Another similar result is found in a model comparison study by Wrightson and Tagliabue (2020), where the only model that had a strong increase in N_2 fixation (58 Tg N yr^{-1}) between years 1800 and 2100 was a model with neither iron nor phosphate limitation on (diagnosed) N_2 fixation. However, two models with neither iron nor explicit diazotrophs in their study showed large decreases in N_2 fixation (38.8 – $50.1 \text{ Tg N yr}^{-1}$) over this time period, due to the tight spatial coupling in the upwelling zones between increasing phosphate limitation, reducing denitrification rates, and the subsequently diagnosed nitrogen fixation (where nitrate is restored to the Redfield ratio). As in our study, models compared in Wrightson and Tagliabue (2020), which include a representation of iron limitation project no substantial change in marine nitrogen fixation (a slight increase by up to 0.4 Tg N yr^{-1}) to decreasing N_2 fixation (up to $23.2 \text{ Tg N yr}^{-1}$). For iron-limited models, they attribute discrepancies across simulated global N_2 fixation trends to differences in the balance between decreasing fixation rates in the Atlantic and Indian Ocean sectors (for which their model ensemble shows a high degree of agreement) and fixation trends in the tropical Pacific sector (for which their model ensemble disagrees on both magnitude and sign). J. K. Moore and Doney (2007) demonstrated that iron stress in diazotrophs have a mitigating effect on global nitrogen cycle responses to perturbation by limiting the ability of diazotrophs to fix nitrogen when upstream denitrification is enhanced, with stabilizing feedbacks between N_2 fixation and denitrification operating least efficiently in the tropical Pacific.

3.3. Simulated Eastern Tropical Pacific Ecosystem Response to Warming

We next look at differences in the model responses to global warming in the ETP, due to its large impact on global N_2 fixation trends (Bonnet et al., 2017; J. K. Moore & Doney, 2007; Wrightson & Tagliabue, 2020 and discussed below). This region has also been previously described as displaying large inter-model differences in nitrogen fixation response to warming (Wrightson & Tagliabue, 2020). Furthermore, Tagliabue et al. (2020) demonstrate biological iron limitation within this region to be of critical importance in determining productivity trends across the equatorial Pacific, which we also suspect to apply to nitrogen fixation trends, based on the global differences between iron-limited models and NoFe, shown above. However, it is also important to note that the different model behavior we report for the ETP also applies to the eastern tropical Atlantic upwelling region. Thus differences in global model trends are not only resulting from differences within the ETP.

As the temperature increases, NPP, remineralization, microbial loop recycling, and other temperature-sensitive fluxes accelerate accordingly (Figure 3). In all models, the surface ocean nutrient recycling pathways through enhanced and shallower detrital remineralization and the enhanced microbial loop gain importance under warming. Also, the increase in phytoplankton potential growth rate is greater than the increase in zooplankton potential grazing rate (which is capped above 20°C ; Keller et al. (2012), in all models). Hence, total plankton biomass (ordinary phytoplankton, diazotrophs and zooplankton) increases in all models in the ETP.

In the NoFe model, light limitation due to phytoplankton self-shading is the dominant control on phytoplankton growth in the ETP (Figure B5). Grazing control on the biomass is also stronger compared to the other models (NoFe has the highest optimized maximum grazing rate at 0°C , see Table B1). With ocean warming, the increase in phytoplankton potential growth rate is larger than the increase in zooplankton potential grazing rate in the ETP. This creates a 23% higher total plankton biomass in the region, which leads to a 35% higher net detritus production (sloppy feeding of zooplankton plus plankton mortality and lysis, minus zooplankton grazing on detritus, Figure 3). Warming also enhances detrital remineralization. However, a 41% increase in detrital remineralization

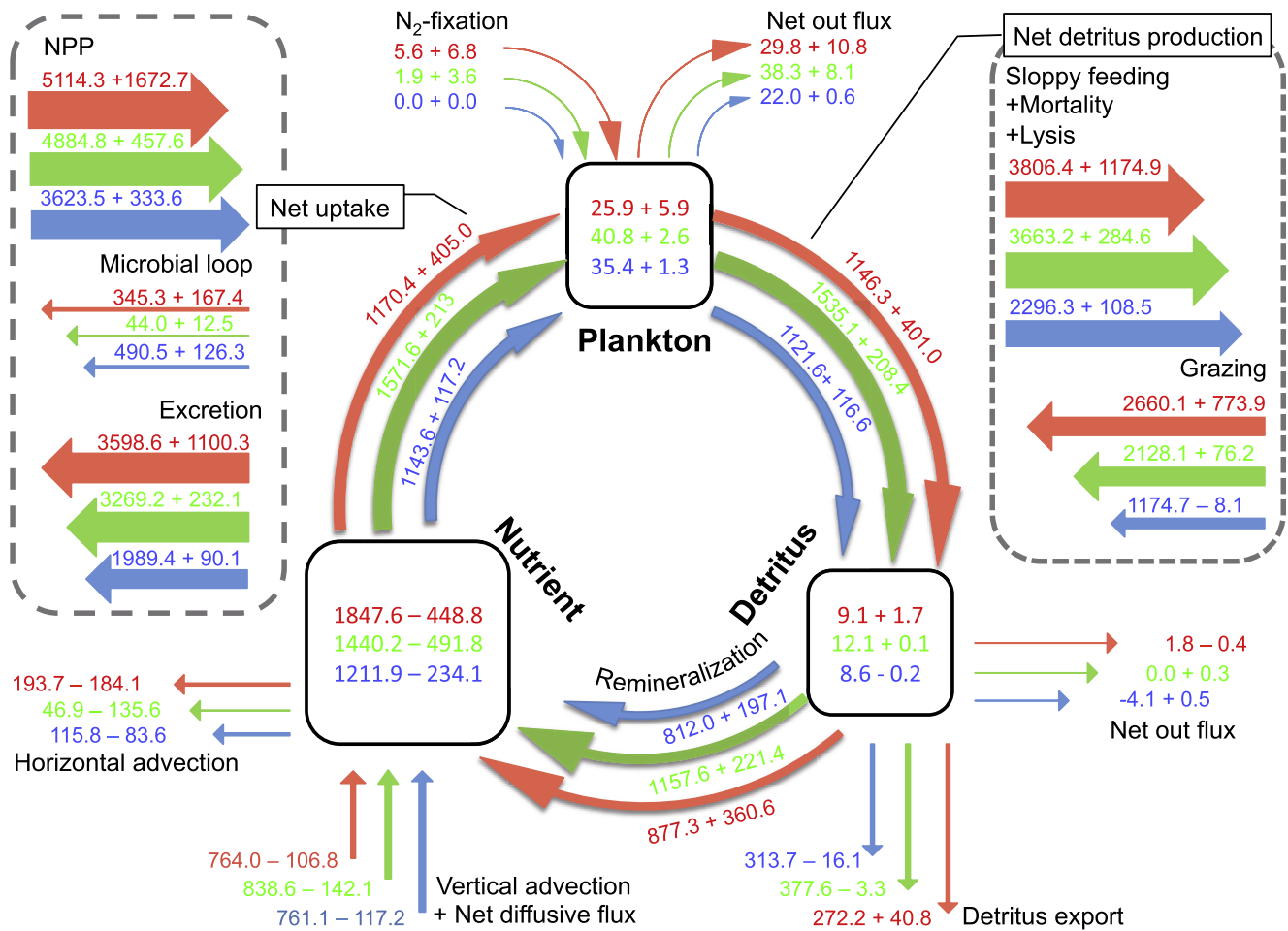


Figure 3. Surface (0–130 m) Surface N cycle (number before + or – sign) and its trend (number after + or – sign) in the Eastern Tropical Pacific (Longitude: 115°W:60°W, Latitude: 8°S:20°N) between years 1800 and 2100. The unit for inventory is Tg C and for fluxes is Tg C yr⁻¹. The thickness of the arrow is approximately proportional to the respective flux. Colors denote different models: NoFe (red), FeMask (green), and FeDyn (blue). Note that all temperature dependent parameters are kept constant across all models so that the different model responses toward warming are the result of different nutrient pathways after model calibration. The parameter list can be found in Table B1.

(Figure 3) is not enough to keep up with the 401.0 Tg C yr⁻¹ increase in net detritus production. Therefore, export production in the ETP increases by 15% (Figure 3), contributing to an increase in the simulated ODZ volume.

Phytoplankton are limited in the ETP by Fe and NO₃ (Figure B5) in both models with iron, which makes their production more sensitive to decreasing nutrient supply under warming-induced intensification of stratification. In FeDyn and FeMask, euphotic zone detrital remineralization accounts for around 23% of the NPP compared to 17.2% in NoFe (Figure 3). Warming increases production in the ETP in FeDyn and FeMask, but also particle remineralization and microbial-loop nutrient recycling. The net effect is a decrease in export production in both models (5.1% for FeDyn and 0.8% for FeMask, Figure 3). The optimized microbial loop constant is larger in FeDyn compared to FeMask (Table B1), and this causes a larger decline in export production in the ETP in this model (Figure 3). In both iron models there is a reduction in ODZ volume in the ETP (Figures B7h and B7i). This different and decreasing trend in ODZ volume in the models with iron has cascading consequences for downstream nitrogen cycling across the tropical Pacific. Reduction of the ODZ volume leads to a decline in total denitrification, which causes water with a relatively greater nitrate-to-phosphate ratio to advect westward. This excess nitrate in the tropical central and western Pacific tends to suppress N₂ fixation by diazotrophs. However, because surface warming also enhances the N₂ fixation rate (see Equation B3), it contributes to the maintenance of N₂ fixation fluxes in FeMask and FeDyn, despite the declining of total denitrification. This decoupling also occurs because according to our model formulation, diazotrophs will always fix some nitrogen (see

Equations B1–B3). Therefore, increasing diazotroph primary production (the drivers of which are discussed in the following section) enhances the N_2 fixation rate in FeMask and FeDyn despite the increasingly unfavorable N:P ratio.

Strong parallels can be found between our results in the ETP and another recent model study: Tagliabue et al. (2020) found that sustained iron limitation in the ETP mitigates future declines in tropical Pacific NPP under global warming, whereas a switch to nitrate limitation could result in large declines in productivity. The driver they identified is different than what we find in our model; they describe a positive feedback in which stratification reduces nitrate resupply, which reduces biomass at the surface and allows deeper light penetration. Greater light levels at depth push the depth of the chlorophyll maximum deeper into the subsurface Equatorial Undercurrent, thereby removing additional nitrate from upwelling water and further reducing surface productivity (Tagliabue et al., 2020). However, if iron remains a stronger control than nitrate on phytoplankton growth (in their experimental setup, achieved by prescribing different biological Fe uptake parameter values), this positive feedback is mitigated by the sustained addition of iron off the South American continent (Tagliabue et al., 2020). As already described, our experimental setup introduces additional differences in nutrient pathways (by different parameter values) beyond sensitivity to biological iron uptake. Still it is interesting to note that even the global NPP trend in our models demonstrates increasing sensitivity to climate change with decreasing ETP iron limitation (comparing Figure 1 and Figure B5), which suggests that controls on phytoplankton growth in this region act as a “gatekeeper” for surface nutrient availability to an extent which can dominate globally averaged responses to warming. This may be a point of concern, as both iron-limited models (as well as others, such as the hand-tuned Nickelsen et al. [2015] and Kvale et al. [2020] variants, as well as CMIP5 models; W. Fu et al., 2016) broadly predict increasing retention of iron in the upper ocean with warming. Regionally, changes in primary production limitation factors into the future in the ETP can produce a cascade of divergent consequences across the tropical Pacific. In Tagliabue et al. (2020), the consequences for NPP and higher trophic levels are described. Here, we explore the consequences for nitrogen cycling. Also similar to our study, Tagliabue et al. (2020) found increasing discrepancies in transient model behavior, and drew their conclusions using a suite of models which performed similarly with respect to NPP over the historical period.

3.4. Decoupling of N_2 -Fixation and Diazotroph Primary Production in Models With Iron

In the NoFe model, we find that increasing N_2 fixation correlates with an increase in diazotroph primary production, which is intuitive as diazotrophs fix N_2 to support their growth when NO_3 is in short supply. In the tropics (30S:30N), global warming increases the temperature-dependent phytoplankton (both diazotrophs and ordinary phytoplankton) potential growth rate and the detritus remineralization rate by around 40% from preindustrial to year 2100, which accelerates surface nutrient cycling and promotes phytoplankton growth in oligotrophic waters. Simulated growth rates in the tropical upwelling zones increase faster under global warming than simulated grazing rates (that are capped at 20°C, see Equation 28 in Keller et al. [2012]), which leads to higher detritus production and then an increase in particle export out of the nutrient-replete upwelling region despite the enhanced remineralization (Figures 3 and 4a), which decreases water column oxygen and increases denitrification (Figures 5a–5c), producing increasingly elevated P^* (Figures 5d–5i) conditions downstream that favor diazotrophs (Figure 6a) and promote N_2 fixation (Figure B4).

However, in FeMask and FeDyn, diazotroph primary production increases over time but N_2 fixation does not. This is because diazotroph primary production and N_2 -fixation can be decoupled (Knapp et al., 2012). In our models, diazotrophs can utilize NO_3 when it is available. Similar to NoFe, surface nutrient cycling is enhanced by warming in the oligotrophic regions for FeMask and FeDyn (including diazotroph primary production). However, persistent iron limitation in the tropical upwelling zones (Figure B5) mitigates the particle export response to regional warming (Figure 4; the net export in the three ODZ regions declines by 66.5 Tg C yr^{-1} for FeMask and 69.0 Tg C yr^{-1} for FeDyn by year 2100). In line with these trends in particle export, a net contraction of the ODZ volume occurs in both models, which reduces total denitrification (Figures 2c, 2d, 5b, and 5c). This decline in denitrification over time results in reduced P^* (Figures 5d, 5e, 5g, and 5i) for the downstream surface ocean, which tends to suppress N_2 fixation associated with the temperature-induced increase in the growth rate of diazotrophs in the stratified, oligotrophic regions. The strength of this effect is subject to model parameter differences. The sensitivity of the modeled denitrification response to changes in water column oxygen depends

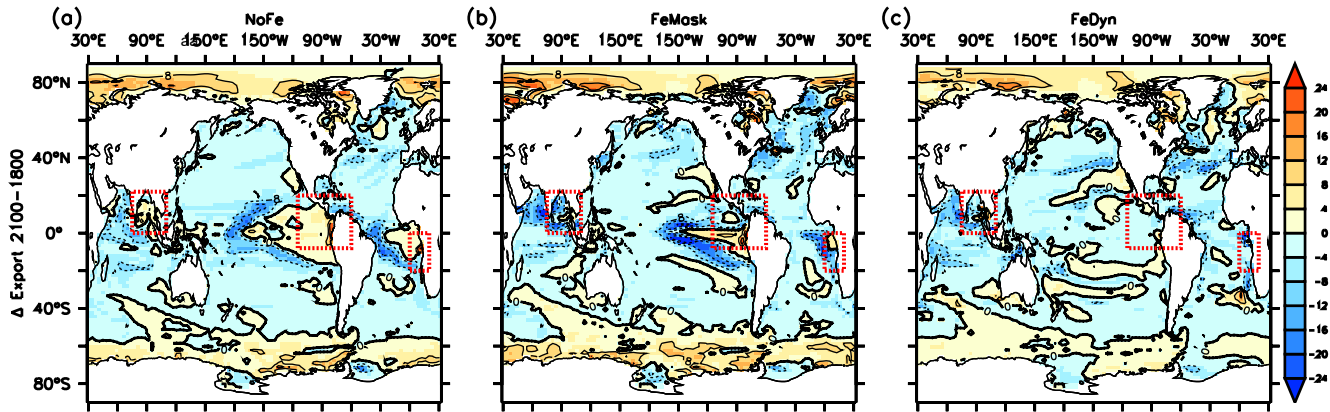


Figure 4. Change in annual export production at 130 m depth (years 2100 minus 1800; from left to right, NoFe, FeMask, FeDyn). Unit for the color scale is $\text{gC m}^{-2} \text{yr}^{-1}$. The solid thick contour line denotes 0, and the solid (dashed) contour denotes positive (negative), the interval is $8 \text{ gC m}^{-2} \text{yr}^{-1}$. The dashed red rectangles represent the Eastern Tropical Pacific, Atlantic and Bay of Bengal regions. Note: the Caribbean region is excluded from the calculations for the box in the Eastern Tropical Pacific.

on the prescribed $\text{O}_2:\text{N}$ ratio, which was determined in the parameter calibrations (Yao et al., 2019) and varies between 9.54 and 10.30 among the models (Table B1). Despite the loss of a competitive advantage over regular phytoplankton due to a declining P^* , diazotrophs are able to maintain a competitive advantage in the oligotrophic regions due to a relative aversion of zooplankton for diazotrophs as a food source (a top-down control; Landolfi et al., 2021). Figures 6a–6f show that the increased diazotroph primary production is usually associated with a higher effective grazing rate on ordinary phytoplankton (more than 0.2 d^{-1} higher compare to the rate on diazotrophs) in the region in the year 2100, for example, the Indian Ocean, the Western Tropical Pacific, and the Tropical Atlantic. This top-down control on ordinary phytoplankton and the temperature-driven increase in growth rates allow diazotrophs to enter regions that are relatively abundant with NO_3^- , where they do not have to fix all the N they need to grow (Figures 6g–6i). This also contributes to the decoupling of the trends of diazotroph NPP and N_2 fixation.

3.5. FeDyn Versus FeMask—Is FeMask a Pragmatic Choice for Climate Projections?

We find no significant differences in the global N_2 fixation trends between the FeDyn and FeMask models over the time period simulated. This similarity in model results may be due to relatively similar parameter values in the two calibrated model versions, or it may be a result of compensating effects keeping surface iron concentrations relatively unchanged under global warming in the dynamic iron model (e.g., iron scavenging and remineralization). While warming enhances remineralization and recycling of iron from particles, iron scavenging and colloid formation can quickly remove the recycled iron from the dissolved phase, which keeps the simulated change in iron concentration under global warming small in the ETP (a 0.4% increase). This small change is not able to qualitatively change the modeled export production in the upwelling zone, hence there is little impact on denitrification and N_2 fixation trends. However, we do see regional differences in other quantities, such as export production trends in the Southern Ocean (Figure 4), which suggest that model-model differences may be regionally significant. In addition, FeMask has prescribed surface iron concentrations, but surface iron concentrations are expected to increase with climate warming (W. Fu et al., 2016), including UVicESCM variants like FeDyn. These dynamic changes are not represented in FeMask, hence the FeDyn model is recommended for climate projections where regional trends are of interest. However if computer resources are limiting and if the focus is on the tropical and subtropical oceans, we can recommend a transient mask of surface dissolved iron concentrations, derived from a single integration of FeDyn, could be applied to FeMask for a physically consistent, but computationally cheaper, representation of iron limitation.

Despite all calibration efforts, it is worth noting that FeDyn also has deficiencies, the most prominent being its poor skill in reproducing observed iron concentrations (Yao et al., 2019). Considering the globally averaged 0.57-year turnover time of iron in FeDyn (compare to other models ranging from a few years to more than 500 years;

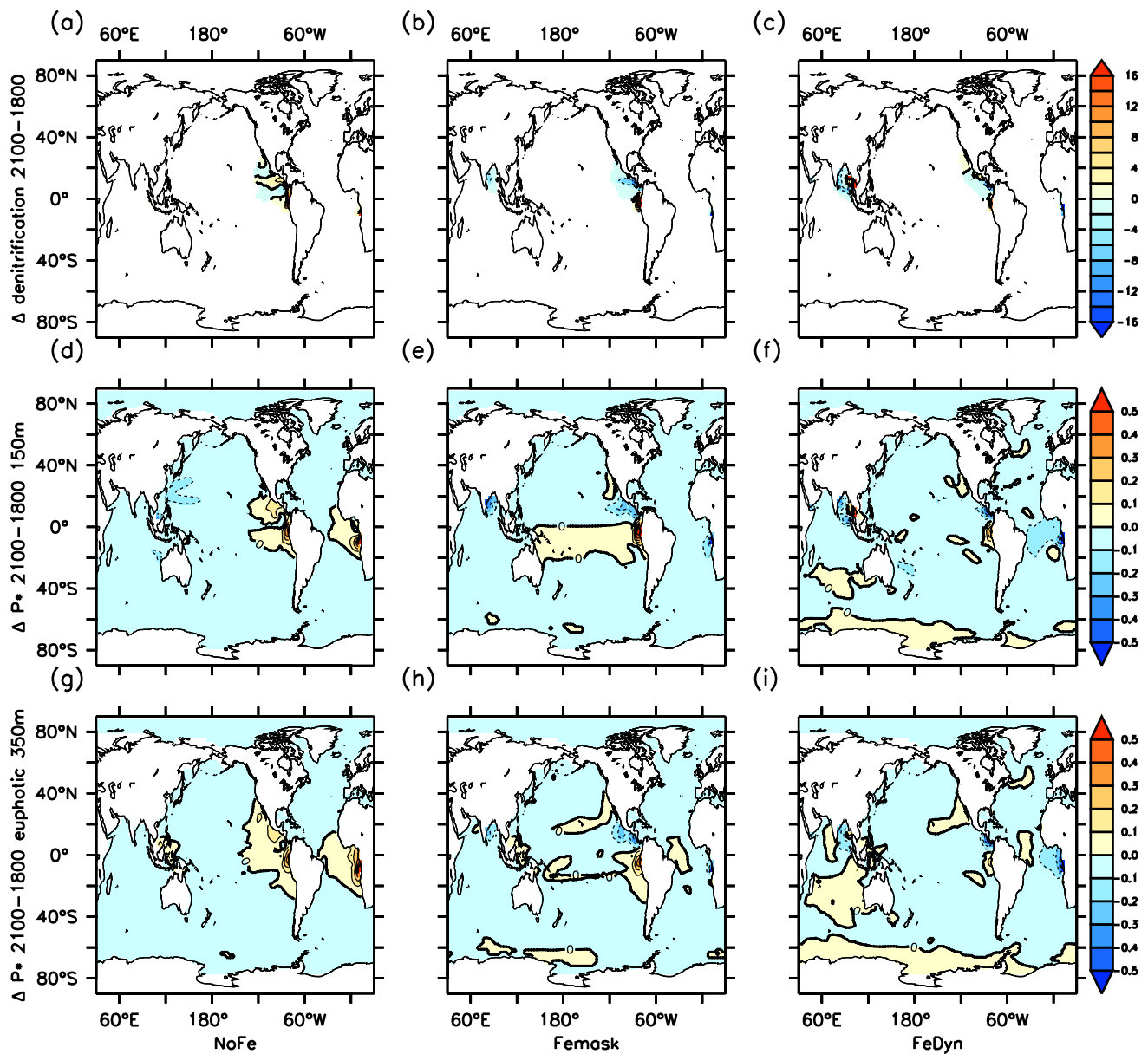


Figure 5. Changes in water column denitrification (top, $\text{gN m}^{-2} \text{yr}^{-1}$), annually averaged P^* concentration (mmol m^{-3}) at 150 m (middle), and 350 m depth (bottom) between years 1800 and 2100. The solid thick contour line denotes 0, and the solid (dashed) contour denotes positive (negative) values. In the top three panels, the contour interval is $4 \text{ gN m}^{-2} \text{yr}^{-1}$, and in the panels (d–i) the contour interval is 0.1 mmol m^{-3} . While PO_4 and NO_3 were used as data constraints in the prior model calibration study (Yao et al., 2019), P^* itself was not.

Tagliabue et al., 2016), the dissolved iron concentration depends strongly on local iron sources, for example, dust deposition, sediment release, and hydro-thermal activity. Sediment release is the largest iron source in our model and a better parameterization for the sediment release might be beneficial for reproducing observed iron concentrations. A recent laboratory study showed that certain types of diatoms can reduce their iron requirement under higher temperatures and maintain their growth rate (Jabre & Bertrand, 2020). This finding suggests a more flexible, even a temperature dependent iron demand. Appropriate parameterizations should be tested in future studies. Likewise, the Fe dust deposition is projected to increase in the future (Hamilton et al., 2020), which we did not account for in this study. The more straightforward option to include more realistic parameterizations of climate-sensitive iron dynamics as well as time-dependent external Fe sources, might shift the balance between the two iron models in favor of FeDyn.

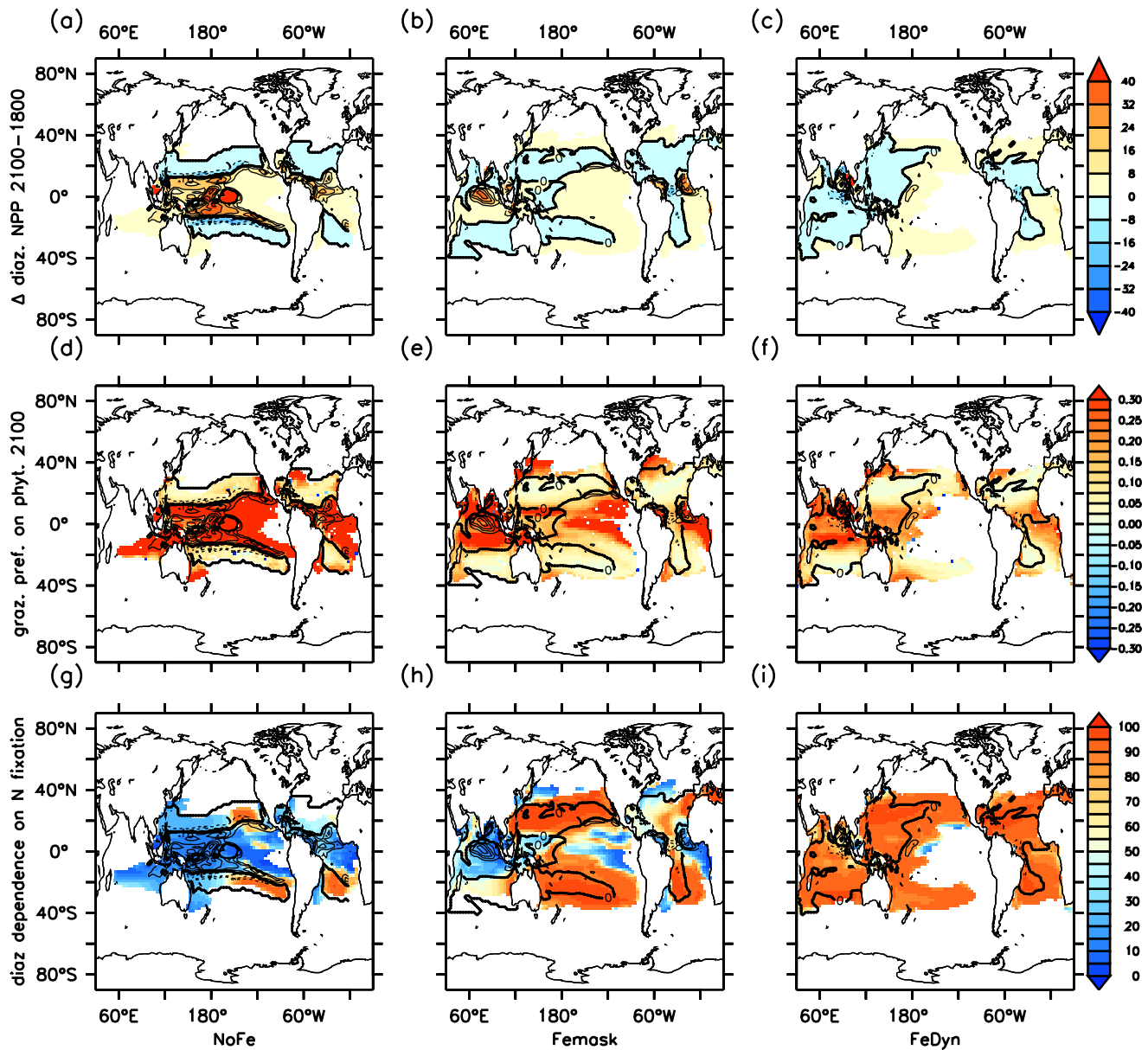


Figure 6. The change in diazotroph NPP (top, $\text{gC m}^{-2} \text{yr}^{-1}$), the preferential grazing pressure on ordinary phytoplankton (middle, d^{-1}), and the percentage of diazotroph growth depending on nitrogen fixation (bottom, %) in three models. The contour lines represent the change in diazotroph NPP in all panels, and the solid thick contour line denotes 0, and the solid (dashed) contour denotes positive (negative). The contour interval is $8 \text{ gC m}^{-2} \text{yr}^{-1}$. The preferential grazing pressure on ordinary phytoplankton is calculated as the effective grazing rate on ordinary phytoplankton minus the effective grazing rate on diazotrophs. The percentage of diazotroph growth depending on nitrogen fixation is a number between 0 and 100, where 0 means that diazotrophs only take up nitrogen from surrounding water for their growth and 100 means that diazotrophs use solely newly fixed nitrogen for its growth. Note that 0 percent dependence on N_2 fixation cannot be reached due to the formulation of diazotroph nitrogen uptake (see Equation B1).

There are still other factors beyond iron parameterization which might further improve the representation of nitrogen cycling in our model. Wrightson and Tagliabue (2020) compiled a list of non-iron-model related potentially significant drivers of N_2 fixation, including CO_2 fertilization of diazotrophs, and a possible upper thermal threshold for optimal growth for phytoplankton, which are not yet implemented in our model and should be explored in the future.

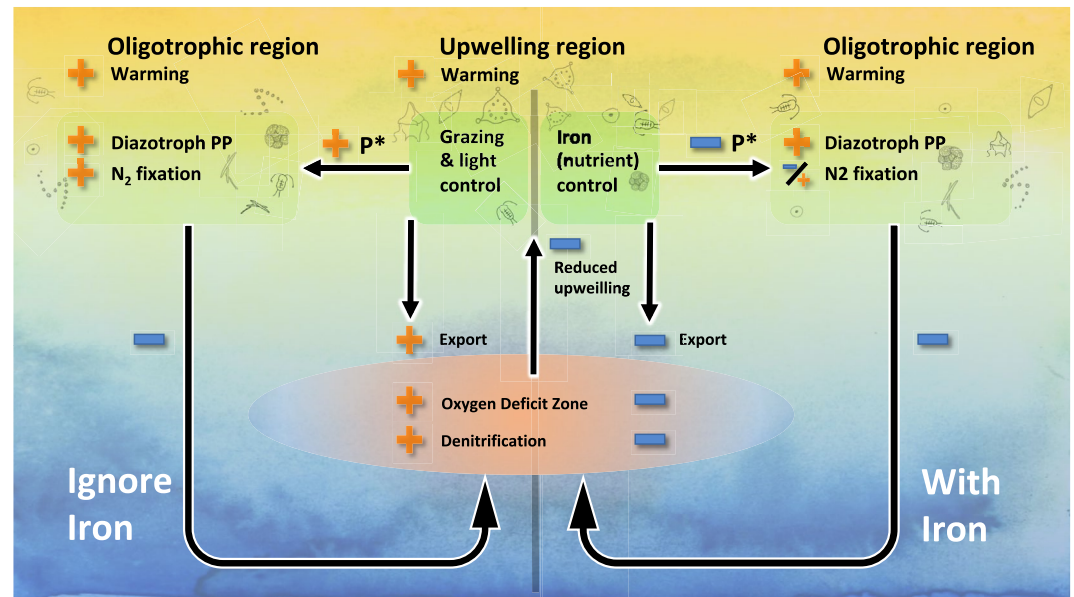


Figure 7. A comparison of two different model responses to tropical warming and water column stratification, with (right side) and without (left side) explicit consideration of iron limitation. The upwelling ecosystem is controlled by a combination of top-down grazing and light limitation when iron does not limit primary production (left side). As the temperature increases, upwelling is reduced (“–” in the center of the figure). In the scenario not considering iron (left part of the figure) primary production increases faster than grazing pressure, which leads to increased particle export (+) and higher remineralization (+). Higher temperatures and increased remineralization intensify water column ODZs (+) and associated denitrification (+). Elevated denitrification leads to higher N_2 fixation, and an increase in diazotroph primary production downstream (+). However, including iron limitation (right side) mitigates the export production response to warming in the upwelling ecosystem. Export production declines (–), and the ODZ volume also shrinks (–). More oxygen in the water column leads to less denitrification (–) and reduced P^* , which suppresses N_2 fixation downstream (–/+ , no apparent change) despite temperature-driven increases in diazotroph primary production.

4. Conclusions

The results presented here demonstrate divergent trends in simulated future global N_2 fixation and denitrification that are determined by the representation of bottom-up and top-down phytoplankton growth limitation in tropical upwelling regions (schematic in Figure 7). When iron limitation is neglected, warming induces positive feedbacks of enhanced regional export production and denitrification that triggers enhanced N_2 fixation across the central and western basin. When iron limitation is accounted for, the response of export production to warming is muted and even produces a net decline in denitrification in the ETP, leading to essentially no apparent change in global marine N_2 fixation.

While the simulated responses of N_2 fixation diverge between the three models tested, all models simulate an increase (albeit, of variable magnitude) in diazotroph primary production. That the N_2 fixation trends hinge upon the treatment of iron limitation in the tropical upwelling zones, but simulated primary production of diazotrophs does not highlight the importance of model structure for simulated future trends. This finding goes beyond J. K. Moore and Doney (2007) in that our simulations do not explore global responses to the presence or absence of diazotroph iron limitation, but instead consider a suite of ecosystem pathway differences in models that perform similarly in steady-state. By using the same physical base model, we are able to isolate and compare ecological pathway responses (which is not possible using multi-model ensembles, e.g., Wrightson & Tagliabue, 2020). Our analysis suggests flux and rate data may be just as (or even more) relevant for calibrating models as are data of biogeochemical tracer concentrations. It also implies that a different choice in calibration objective (say, application of a mix of flux and nutrient distribution data), or weighting of surface versus deep ocean attributes, or a different choice of parameter sets, could produce alternative optimal parameter sets with unique transient behaviors. However, we expect that even with different ecosystem structures, the same basic relationship between ETP iron limitation and global N_2 fixation response will apply, as Tagliabue et al. (2020) demonstrated a similar

effect in their model ensemble for tropical NPP. An interesting additional test, which we leave to the future, would be to explore the role of model parameter choice in long-term recovery from the decoupling between diazotroph primary production and nitrogen fixation.

Our finding of a strong connection between global N_2 fixation rates and iron limitation in upwelling zones sheds new light on two controlling factors of N_2 fixation, namely iron limitation and denitrification. From a global view, spatial patterns of N_2 fixation are not only controlled by iron availability in oligotrophic regions (as proposed by Ward et al. [2013]), but also by the iron limitation upstream, which regulates the denitrification (and hence, P^*) pattern. Lastly, our study demonstrates a role of temperature in determining N_2 fixation perturbation patterns. In our earlier study we demonstrated a correlation between denitrification and N_2 fixation as well as globally balanced rates in all model steady states (Yao et al., 2019). However, this linkage is reduced in transient conditions, such as ongoing climate warming. As temperature increases, temperature-sensitive rates regulating bottom-up and top-down controls on export production respond differently. The net result is a decreasing sensitivity of N_2 fixation to denitrification (seen particularly in the models with iron) that can lead to at least a temporary imbalance in global rates. Furthermore, there is growing evidence that heterotrophs may play a role in N_2 fixation (Moisander et al., 2017), and that N_2 fixation in key cyanobacterial diazotrophs may not be stimulated by the lack of NO_3 (Mills et al., 2020). Both of these factors might contribute further to the spatial decoupling between N_2 fixation, and denitrification, and the temporal and spatial decoupling of N_2 fixation and diazotroph primary production which might operate on decadal and longer timescales (J. K. Moore & Doney, 2007). The long-term implications of potential N_2 fixation and denitrification imbalance would be an interesting topic worthy of further study.

This study has shown that even models that are calibrated essentially equally well to global compilations of biogeochemical tracer distributions in an assumed seasonally cycling climatological state, can lead to quantitatively and qualitatively different projections of key biogeochemical processes like nitrogen fixation in transient global warming simulations. Until there are sufficient observations to constrain the sensitivity of transient model simulations to environmental change, it will remain difficult to estimate uncertainties of model projections. Further developing, testing and applying mechanistically sound representations of relevant model features, such as the marine iron cycle and marine nitrogen fixation can be a promising way forward to reduce uncertainties. This may work best when the calibration process can be extended to include large-amplitude historical variability that may resolve part of the sensitivity of marine biogeochemistry to changes in the environment.

Appendix A: Nutrient and Light Limitation on Phytoplankton Growth

The nutrient limitation factor is defined in the model as a function of nutrient concentration and phytoplankton nutrient uptake half-saturation rate:

$$X_{Lim(O\ or\ D)} = \frac{C_X}{C_X + k_{X(O\ or\ D)}}, \quad (A1)$$

X is NO_3 , PO_4 or Fe , C_X is the concentration of X and $k_{X(O\ or\ D)}$ is the phytoplankton half-saturation of the uptake rate for X . Light limitation is derived from Keller et al. (2012, for NoFe and FeMask) and Nickelsen et al. (2015, for FeDyn) as:

$$L_{lim(O\ or\ D)} = \frac{\alpha_{(O\ or\ D)} I}{\sqrt{\left(J_{max(O\ or\ D)}^2 + (\alpha_{(O\ or\ D)} I)^2\right)}} \quad (A2)$$

where $\alpha_{(O\ or\ D)}$ is the initial slope of the photosynthesis-irradiance curve (in FeDyn, $\alpha_{(O\ or\ D)}$ is dependent on $Fe_{Lim(O\ or\ D)}$, details see Nickelsen et al., 2015), I is the in situ irradiance and $J_{max(O\ or\ D)}$ is the in situ maximum potential growth rate.

$$J_{max(O\ or\ D)} = a \cdot F_{temp(O\ or\ D)} \quad (A3)$$

a is the phytoplankton growth rate constant at 0°C. $F_{temp(O\ or\ D)}$ is a temperature factor for biological process.

$$F_{tempO} = \exp(T/T_b) \quad (A4)$$

$$F_{tempD} = Cd \cdot \max(0, a(\exp(T/T_b) - 2.61)) \quad (A5)$$

T is the situ temperature and T_b is the e-folding temperature of biological rates, C_d is a handicap for diazotroph growth and the 2.61 temperature scaling is to inhibit diazotrophs growth below 15°C.

The iron is not incorporated in the nutrient minimum function but as a factor that directly governs the growth rate. The in situ growth rate of ordinary phytoplankton (J_O) and diazotrophs (J_D) are defined as:

$$J_O = \min(NO_{3limO}, PO_{4limO}, L_{limO}) \cdot Fe_{LimO} \cdot a \cdot F_{tempO} \quad (A6)$$

$$J_D = \min(PO_{4limD}, L_{limD}) \cdot Fe_{LimD} \cdot a \cdot F_{tempD} \quad (A7)$$

More details of model equations can be found in Keller et al. (2012, FeMask and NoFe) and Nickelsen et al. (2015, FeDyn).

Appendix B: Nitrogen Fixation by Diazotrophs

As described in Schmittner et al. (2008), the diazotrophs can take up nitrogen from the surrounding water when it is available, and it can fix nitrogen when the preformed nitrogen does not satisfy the demand for growth. The growth rate for diazotrophs is described in Equation A7, and does not depend on preformed nitrogen concentration in the water. The nitrogen uptake rate from the surrounding water is described as in Schmittner et al. (2008) as (Table B1; Figures B1, B2, B3, B4, B5, B6, and B7):

$$J_{NO_3D} = \frac{C_{NO_3}}{C_{NO_3} + k_N} J_D, \quad (B1)$$

Table B1

The Biogeochemical Parameter Values for Each Model, Resulting From an Objective Calibration Focused on a Sub-Set of Parameters

| Parameter | Description | NoFe | FeMask | FeDyn | Units |
|---------------------------------|--|---------------------|---------------------|--------|---|
| 1. Phytoplankton (P_O, P_D) | | | | | |
| a | Maximum growth rate parameter at 0°C | 0.698 ^a | 0.6 | 0.6 | d^{-1} |
| m_{P_O} | P_O mortality rate | 0.03 | 0.03 | 0.03 | d^{-1} |
| μ_P^* | Microbial loop constant | 0.0157 ^a | 0.0012 ^a | 0.015 | d^{-1} |
| c_D | Diazotrophs' handicap | 0.4 | 0.4 | 0.4 | |
| Light limitation | | | | | |
| k_w | Light attenuation due to water | 0.04 | 0.04 | 0.04 | m^{-1} |
| k_c | Light attenuation through phytoplankton | 0.047 | 0.047 | 0.047 | $m^{-1} (mmol N m^{-1})^{-1}$ |
| k_i | Light attenuation through sea ice & snow | 5.0 | 5.0 | 5.0 | m^{-1} |
| PAR | Fraction of photosynthetically active radiation | 0.43 | 0.43 | 0.43 | |
| θ_{min} | Maximum Chl:C ratio, extreme iron limitation | | 0.01 | 0.01 | $g Chl (g C)^{-1}$ |
| θ_{max} | Maximum Chl:C ratio, abundant iron | | 0.04 | 0.04 | $g Chl (g C)^{-1}$ |
| α | Initial slope of the P-I curve | | 0.1 | 0.1 | $(W m^{-2})^{-1} d^{-1}$ |
| α_{min} | Minimum chlorophyll specific initial slope in PI-curve | | | 18.4 | $\mu g C (g Chl)^{-1} (W m^{-2})^{-1} s^{-1}$ |
| α_{max} | Maximum chlorophyll specific initial slope in PI-curve | | | 73.6 | $\mu g C (g Chl)^{-1} (W m^{-2})^{-1} s^{-1}$ |
| Macro-nutrient limitation | | | | | |
| K_N | Half saturation constant for N uptake | 0.7 | 0.7 | 0.7 | $mmol N m^{-3}$ |
| $R_{P:N}$ | Molar P:N ratio | 0.0625 | 0.0625 | 0.0625 | |

Table B1

Continued

| Parameter | Description | NoFe | FeMask | FeDyn | Units |
|----------------------------------|--|---------------------|--------------------|---------------------|--------------------------------------|
| K_P | Half saturation constant for P uptake | $K_N R_{P:N}$ | $K_N R_{P:N}$ | $K_N R_{P:N}$ | $\mu\text{mol m}^{-3}$ |
| Iron limitation | | | | | |
| K_{Fe}^P | Half-saturation constant for P_O iron limitation | | 0.05 ^a | | $\mu\text{mol Fe m}^{-3}$ |
| $K_{Fe}^{P\ min}$ | Minimum K_{Fe}^P | | | 0.04 | $\mu\text{mol Fe m}^{-3}$ |
| $K_{Fe}^{P\ max}$ | Maximum K_{Fe}^P | | | 0.406 ^a | $\mu\text{mol Fe m}^{-3}$ |
| P_{max} | P_O biomass above which K_{Fe}^P increases | | | 0.15 | mmol N m^{-3} |
| K_{Fe}^D | Half-saturation constant for Diaz Iron limitation | | 0.406 ^a | 0.377 ^a | $\mu\text{mol Fe m}^{-3}$ |
| $R_{Fe:N}$ | Molar Fe:N ratio for iron uptake | | | 66.25 | $\mu\text{mol Fe (mol N)}^{-1}$ |
| 2. Zooplankton (Z) | | | | | |
| g_Z^0 | Maximum grazing rate at 0°C | 1.282 ^a | 0.668 ^a | 0.567 ^a | d^{-1} |
| g_Z^e | Z growth efficiency | 0.4 | 0.4 | 0.4 | |
| γ | Z assimilation efficiency | 0.7 | 0.7 | 0.7 | |
| m_Z | Z quadratic mortality | 0.06 | 0.06 | 0.06 | $(\text{mmol N m}^{-3})^{-2} d^{-1}$ |
| K_{Graz} | half-saturation constant for Z grazing | 0.15 | 0.15 | 0.15 | mmol N m^{-3} |
| ψ_{P_O} | Z preference for P_O | 0.3 | 0.3 | 0.3 | |
| ψ_{P_D} | Z preference for P_D | 0.1 | 0.1 | 0.1 | |
| ψ_Z | Z preference for other Z | 0.3 | 0.3 | 0.3 | |
| ψ_{Det} | Z preference for <i>Det</i> | 0.3 | 0.3 | 0.3 | |
| 3. Detritus (Det) | | | | | |
| μ_{Det}^0 | <i>Det</i> remineralization rate at 0°C | 0.055 | 0.055 | 0.055 | |
| ω_{Det}^0 | Sinking speed of <i>Det</i> at surface | 14 | 14 | 14 | m d^{-1} |
| ω_{Det}^j | Depth dependent sinking speed slope | 0.065 ^a | 0.062 ^a | 0.060 ^a | d^{-1} |
| Carbonate | | | | | |
| $R_{C:N}$ | Molar C: N ratio | 6.625 | 6.625 | 6.625 | |
| $R_{CaCO_3:POC}$ | CaCO ₃ over nonalgal POC production ratio | 0.03 | 0.03 | 0.03 | |
| D_{CaCO_3} | CaCO ₃ remineralization e-folding depth | 6,500 | 6,500 | 6,500 | <i>m</i> |
| 4. Iron (Fe) | | | | | |
| L_T | Total ligand concentration | | | 1 | $\mu\text{mol lig m}^{-3}$ |
| K_{FeL} | Fe-ligand stability constant | | | 10 ^{5.5} | $(\text{mmol lig m}^{-3})^{-1}$ |
| $R_{Fe:P\ sed}$ | Molar Fe: P for sedimentary iron source | | | 0.004 | |
| $O_2\ min$ | Minimum O ₂ concentration for aerobic oxidation | 5 | 5 | 5 | $\text{mmol O}_2\ \text{m}^{-3}$ |
| K_{Fe}^{org} | Organic-matter dependent scavenging rate | | | 0.427 ^a | |
| $K_{Fe}^{org\ s}$ | Organic-matter particle scaling for scavenging | | | 0.58 | |
| K_{Fe}^{col} | Fe colloidal production and precipitation rate | | | 0.005 | d^{-1} |
| 5. Oxygen (O₂) | | | | | |
| $R_{O:N}$ | Molar O: N ratio | 10.439 ^a | 9.541 ^a | 10.502 ^a | |
| 6. Temperature dependency | | | | | |
| <i>b</i> | Scaling factor <i>b</i> for temperature dependent process | 1.066 | 1.066 | 1.066 | |
| <i>c</i> | Scaling factor <i>c</i> for temperature dependent process | 1.0 | 1.0 | 1.0 | $(^\circ\text{C})^{-1}$ |

Note. For computational and conceptual reasons, the number of tuneable parameters had to be constrained to a relatively small number. We selected those parameters that showed largest impact on the model results as shown in Yao et al. (2019). The microbial loop constant describes the rate of bacteria (not explicit modeled) recycling the phytoplankton biomass back to the resolved nutrient pool. The diazotrophs' handicap means that the diazotrophs maximum growth rate is around 40% of ordinary phytoplankton (*a*). For more details of the parameter of the model, please see Keller et al. (2012) and Nickelsen et al. (2015).

^aParameter value optimized for the model.

where C_{NO_3} is the nitrate concentration in the water, and k_N is the half saturation constant for N uptake. Hence the N_2 fixation rate is:

$$R_{fix} = \left(1 - \frac{C_{NO_3}}{C_{NO_3} + k_N}\right) J_D, \quad (B2)$$

$$R_{fix} = \left(1 - \frac{C_{NO_3}}{C_{NO_3} + k_N}\right) \cdot \min(PO4_{limD}, L_{limD}) \cdot Fe_{LimD} \cdot a \cdot F_{tempD}. \quad (B3)$$

More details of the model equation for N_2 fixation can be found in Schmittner et al. (2008).

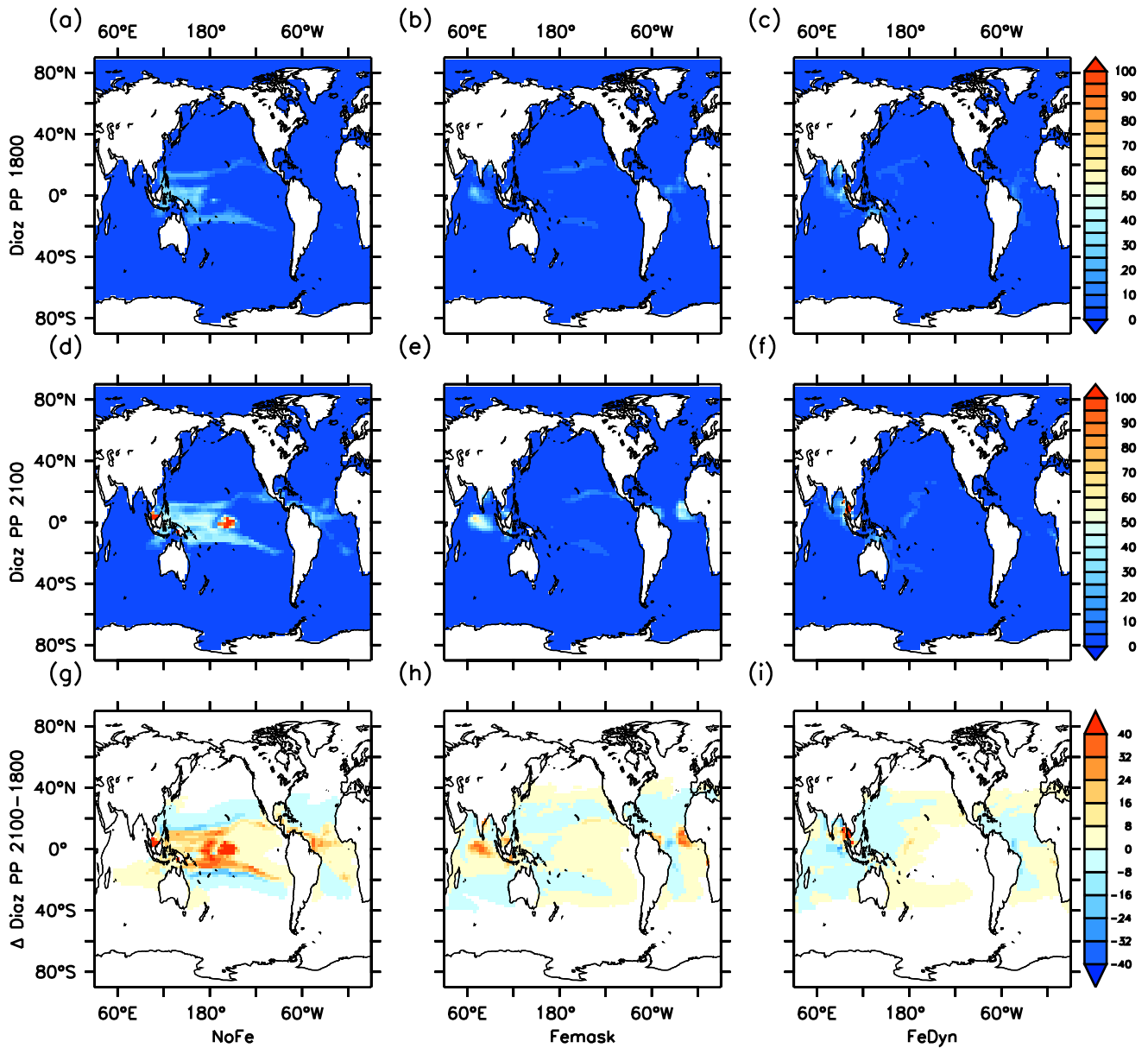


Figure B1. Diazotrophs primary production in the year 1800 (upper), in the year 2100 (middle), and their differences (lower) for three models. The unit is $gC\ m^{-2}\ yr^{-1}$.

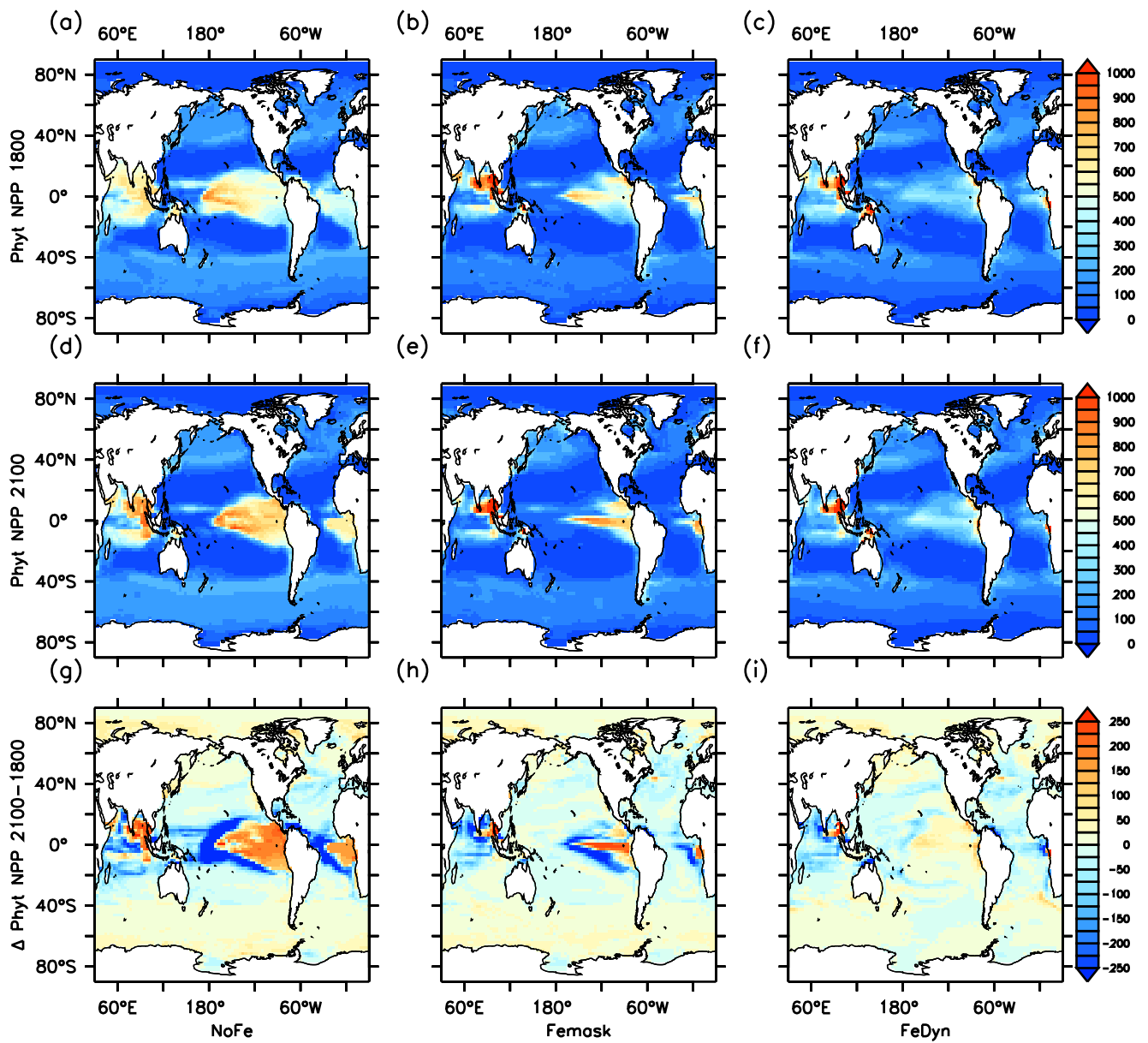


Figure B2. Ordinary phytoplankton NPP in the year 1800 (upper), in the year 2100 (middle), and their differences (lower) for three models. The unit is gC m⁻² yr⁻¹.

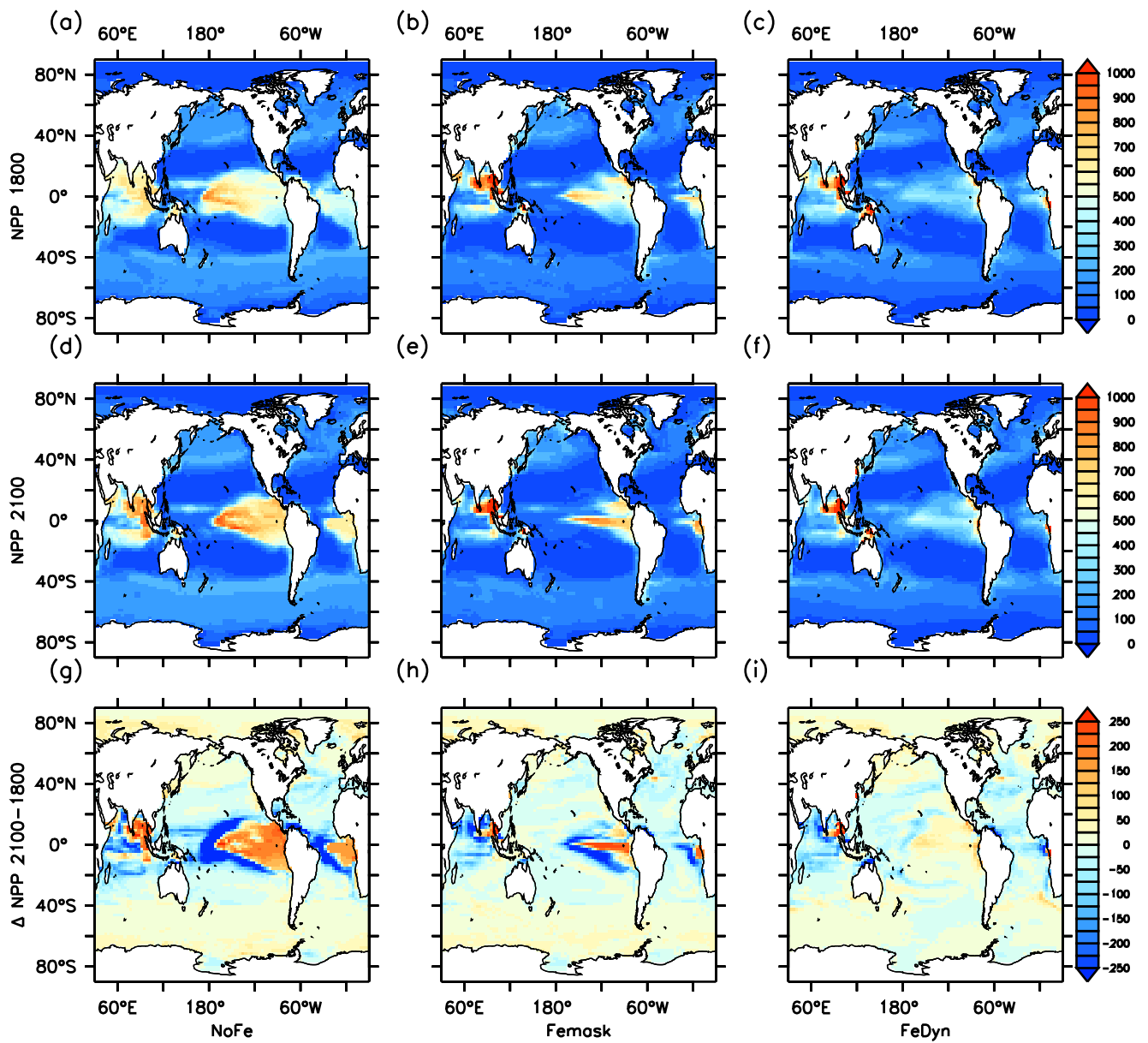


Figure B3. Total NPP in the year 1800 (upper), in the year 2100 (middle), and their differences (lower) for three models. The unit is $\text{gC m}^{-2} \text{yr}^{-1}$.

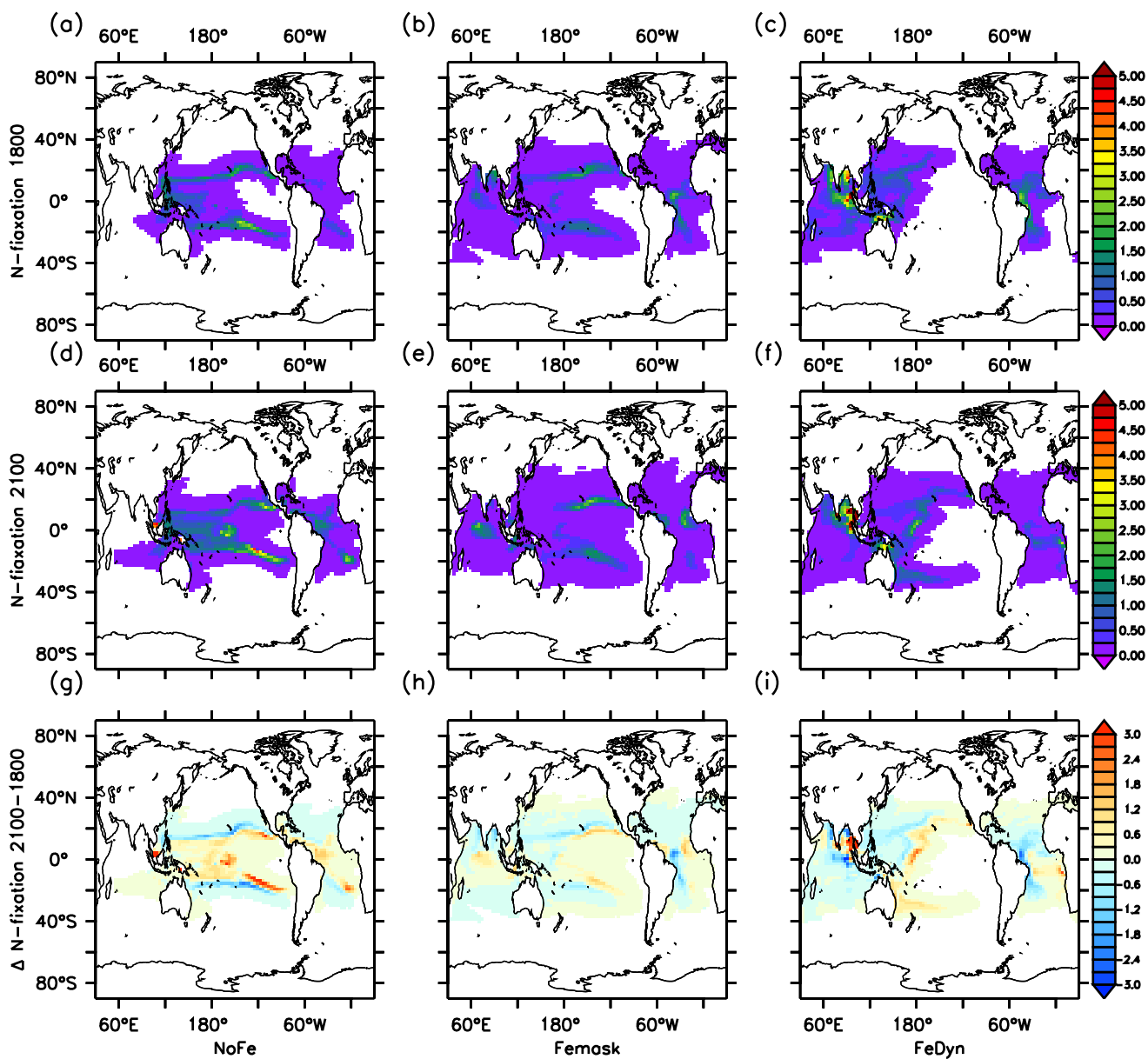


Figure B4. Nitrogen fixation in the year 1800 (upper), in the year 2100 (middle), and their differences (lower) for three models. The unit is $\text{gN m}^{-2} \text{yr}^{-1}$.

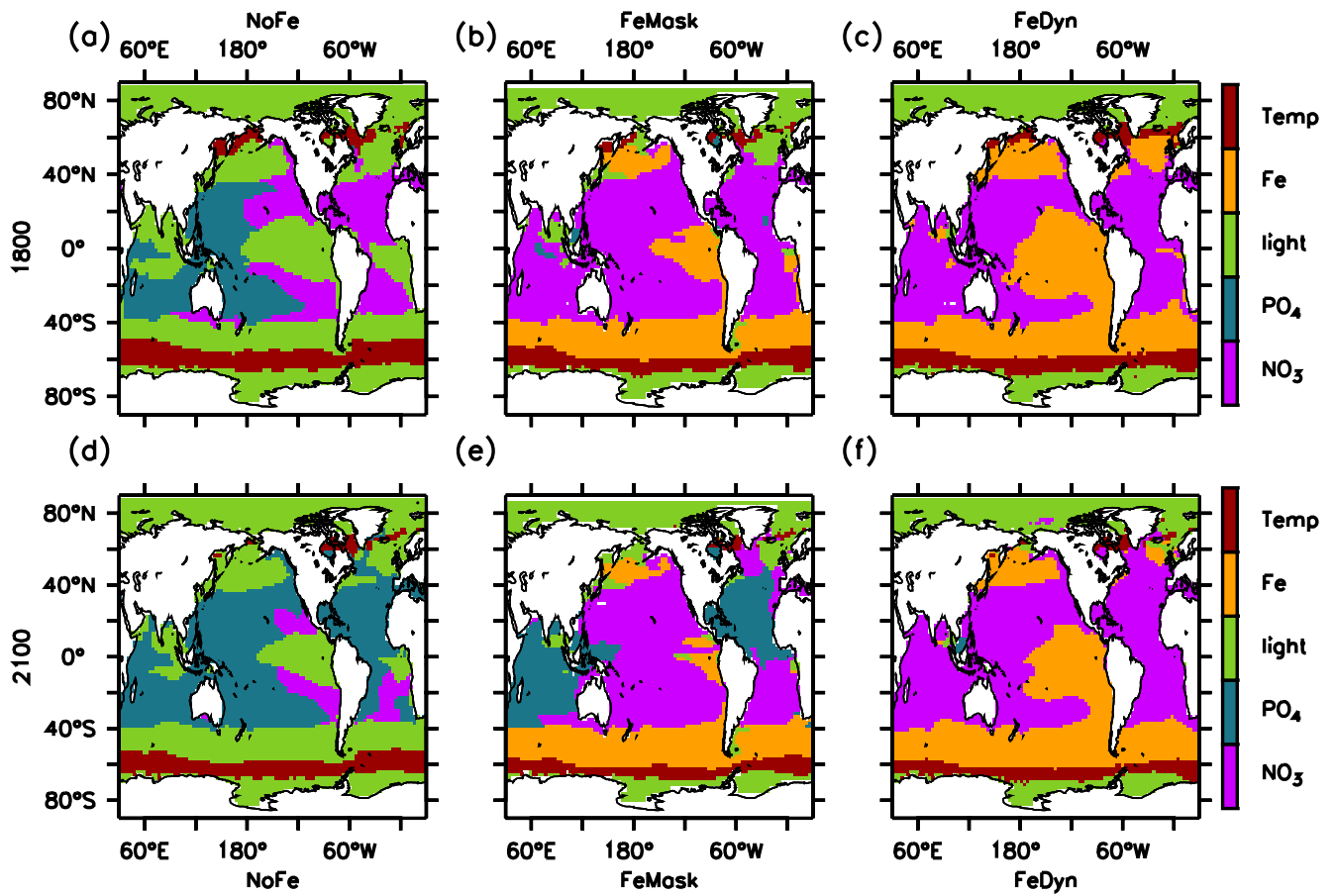


Figure B5. The most limiting growth factor for ordinary phytoplankton in all models in the years 1800 (upper) and 2100 (lower).

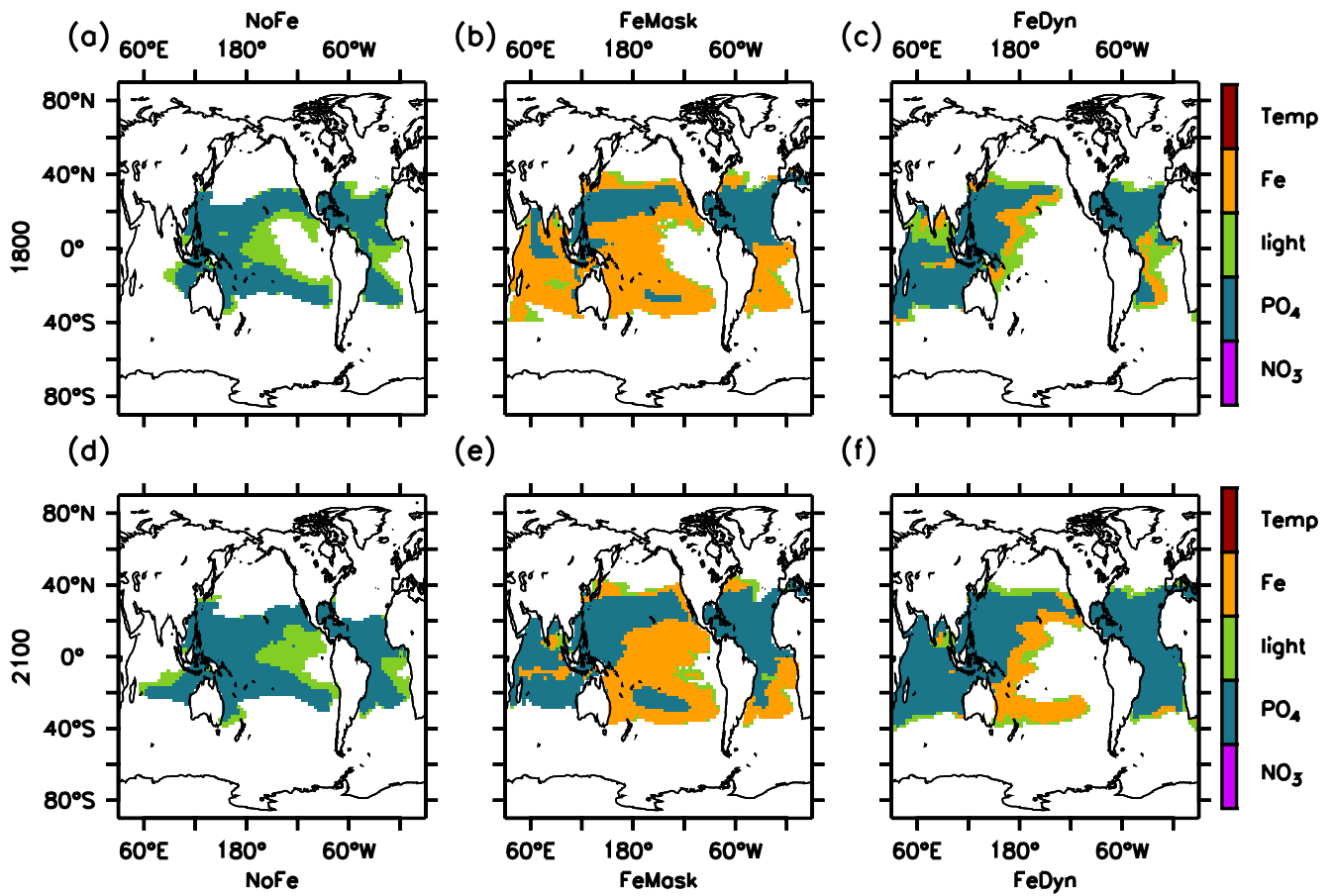


Figure B6. The most limiting growth factor for diazotrophs in all models in the years 1800 (upper) and 2100 (lower).

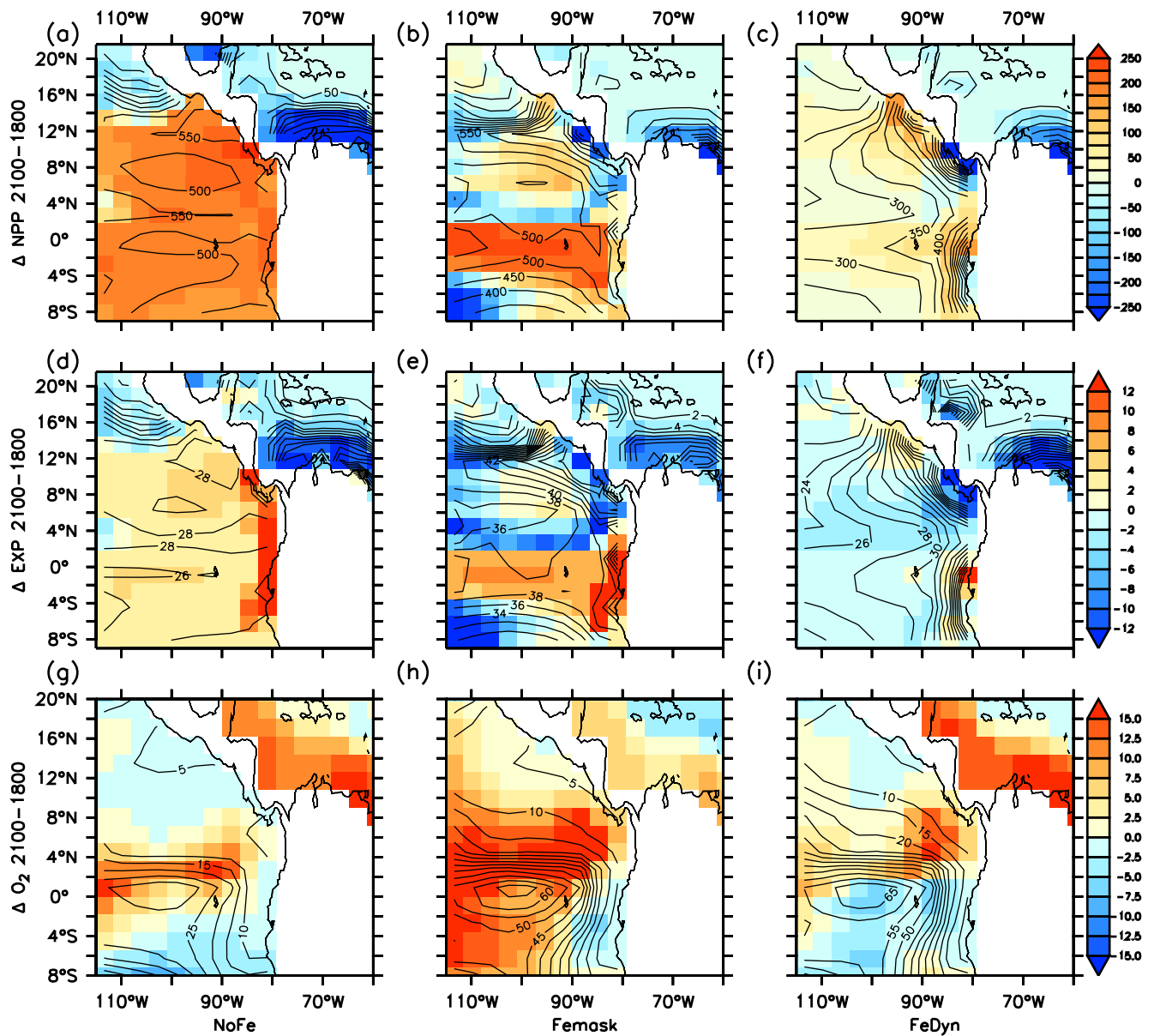


Figure B7. Annually averaged total NPP, export, and oxygen concentration (depth 350 m) in the Eastern Tropic Pacific. Color shading represents the difference between year 2100 and 1800 and contours show simulated values in year 2100. The unit for NPP and export production is $\text{g C m}^{-2} \text{yr}^{-1}$ and the unit for O_2 concentration is mmol m^{-3} . The interval between neighboring lines are $50 \text{ g C m}^{-2} \text{yr}^{-1}$ for NPP, $2 \text{ g C m}^{-2} \text{yr}^{-1}$ for export, and 5 mmol m^{-3} for O_2 .

Data Availability Statement

Model code and model data used in writing this manuscript are available on OceanRep—GEOMAR Repository (<https://data.geomar.de/downloads/20.500.12085/673e7de0-20ab-4dd3-afe9-c4bf00b1faf/>).

Acknowledgments

The authors would like to acknowledge computer resources from Christian-Albrechts-University of Kiel (CAU) and GEOMAR Helmholtz Centre for Ocean Research, Kiel. This work is supported by the Helmholtz Research School for Ocean System Science and Technology (HOSST, Germany) at GEOMAR Helmholtz Centre for Ocean Research Kiel (VH-KO-601). K. Kvale acknowledges support from GEOMAR Helmholtz Centre for Ocean Research Kiel and the New Zealand Ministry of Business, Innovation and Employment through the Global Change through Time Program. All authors are grateful for stimulating discussion within the Biogeochemical Modeling and Marine Chemistry research units at GEOMAR, Dalhousie University, and University of Liverpool. Open access funding enabled and organized by Projekt DEAL.

References

- Bitz, C. M., & Lipscomb, W. H. (1999). An energy-conserving thermodynamic model of sea ice. *Journal of Geophysical Research*, *104*(C7), 15669–15677. <https://doi.org/10.1029/1999JC900100>
- Bonnet, S., Caffin, M., Berthelot, H., & Moutin, T. (2017). Hot spot of N₂ fixation in the western tropical South Pacific pleads for a spatial decoupling between N₂ fixation and denitrification. *Proceedings of the National Academy of Sciences*, *114*(14), E2800–E2801. <https://doi.org/10.1073/pnas.1619514114>
- Bopp, L., Resplandy, L., Orr, J. C., Doney, S. C., Dunne, J. P., Gehlen, M., et al. (2013). Multiple stressors of ocean ecosystems in the 21st century: Projections with CMIP5 models. *Biogeosciences*, *10*(10), 6225–6245. <https://doi.org/10.5194/bg-10-6225-2013>
- Breitbarth, E., Oschlies, A., & LaRoche, J. (2007). Physiological constraints on the global distribution of Trichodesmium - Effect of temperature on diazotrophy. *Biogeosciences*, *4*(1), 53–61. <https://doi.org/10.5194/bg-4-53-2007>
- Buchanan, P. J., Chase, Z., Matear, R. J., Phipps, S. J., & Bindoff, N. L. (2019). Marine nitrogen fixers mediate a low latitude pathway for atmospheric CO₂ drawdown. *Nature Communications*, *10*(1), 1–10. <https://doi.org/10.1038/s41467-019-12549-z>
- Cabr e, A., Marinov, I., & Leung, S. (2015). Consistent global responses of marine ecosystems to future climate change across the IPCC AR5 Earth system models. *Climate Dynamics*, *45*(5–6), 1253–1280. <https://doi.org/10.1007/s00382-014-2374-3>
- Carr, M. E., Friedrichs, M. A., Schmeltz, M., Noguchi Aita, M., Antoine, D., Arrigo, K. R., et al. (2006). A comparison of global estimates of marine primary production from ocean color. *Deep Sea Research Part II: Topical Studies in Oceanography*, *53*(5–7), 741–770. <https://doi.org/10.1016/j.dsr2.2006.01.028>
- Deutsch, C., Sarmiento, J. L., Sigman, D. M., Gruber, N., & Dunne, J. P. (2007). Spatial coupling of nitrogen inputs and losses in the ocean. *Nature*, *445*(7124), 163–167. <https://doi.org/10.1038/nature05392>
- Eby, M., Weaver, A. J., Alexander, K., Zickfeld, K., Abe-Ouchi, A., Cimadoribus, A. A., et al. (2013). Historical and idealized climate model experiments: An intercomparison of Earth system models of intermediate complexity. *Climate of the Past*, *9*(3), 1111–1140. <https://doi.org/10.5194/cp-9-1111-2013>
- Fanning, A. F., & Weaver, A. J. (1996). An atmospheric energy-moisture balance model: Climatology, interpentadal climate change, and coupling to an ocean general circulation model. *Journal of Geophysical Research*, *101*, 15111–15128. <https://doi.org/10.1029/96JD01017>
- Fu, F., Yu, E., Garcia, N., Gale, J., Luo, Y., Webb, E., & Hutchins, D. (2014). Differing responses of marine N₂ fixers to warming and consequences for future diazotroph community structure. *Aquatic Microbial Ecology*, *72*(1), 33–46. <https://doi.org/10.3354/ame01683>
- Fu, W., Randerson, J. T., & Keith Moore, J. (2016). Climate change impacts on net primary production (NPP) and export production (EP) regulated by increasing stratification and phytoplankton community structure in the CMIP5 models. *Biogeosciences*, *13*(18), 5151–5170. <https://doi.org/10.5194/bg-13-5151-2016>
- Galbraith, E. D., Gnanadesikan, A., Dunne, J. P., & Hiscock, M. R. (2010). Regional impacts of iron-light colimitation in a global biogeochemical model. *Biogeosciences*, *7*(3), 1043–1064. <https://doi.org/10.5194/bg-7-1043-2010>
- Garcia, H. E., Locarnini, R. A., Boyer, T. P., Antonov, J. I., Baranova, O. K., Zweng, M. M., et al. (2013a). World Ocean Atlas 2013 Volume 4: Dissolved inorganic nutrients (phosphate, nitrate, silicate). *NOAA Atlas NESDIS*, *76*(4), 27. <https://doi.org/10.7289/V5J67DWD>
- Garcia, H. E., Locarnini, R. A., Boyer, T. P., Antonov, J. I., Mishonov, A. V., Baranova, O. K., et al. (2013b). World Ocean Atlas 2013. Volume 3: Dissolved oxygen, apparent oxygen utilization, and oxygen saturation. In *NOAA Atlas NESDIS* (Vol. 75, p. 27). <https://doi.org/10.7289/V5XG9P2W>
- Garcia, N. S., Fu, F., Sedwick, P. N., & Hutchins, D. A. (2015). Iron deficiency increases growth and nitrogen-fixation rates of phosphorus-deficient marine cyanobacteria. *The ISME Journal*, *9*(1), 238–245. <https://doi.org/10.1038/ismej.2014.104>
- Getzlaff, J., & Dietze, H. (2013). Effects of increased isopycnal diffusivity mimicking the unresolved equatorial intermediate current system in an Earth system climate model. *Geophysical Research Letters*, *40*(10), 2166–2170. <https://doi.org/10.1002/grl.50419>
- Gruber, N., & Galloway, J. N. (2008). An Earth-system perspective of the global nitrogen cycle. *Nature*, *451*(7176), 293–296. <https://doi.org/10.1038/nature06592>
- Hamilton, D. S., Moore, J. K., Arneeth, A., Bond, T. C., Carslaw, K. S., Hantson, S., et al. (2020). Impact of changes to the atmospheric soluble iron deposition flux on ocean biogeochemical cycles in the anthropocene. *Global Biogeochemical Cycles*, *34*(3), 1–22. <https://doi.org/10.1029/2019GB006448>
- Jabre, L., & Bertrand, E. M. (2020). Interactive effects of iron and temperature on the growth of *Fragilariopsis cylindrus*. *Limnology and Oceanography Letters*, *5*, 363–370. <https://doi.org/10.1002/lo2.10158>
- Karl, D., Michaels, A., Bergman, B., Capone, D., Carpenter, E., Letelier, R., et al. (2002). Dinitrogen fixation in the world's oceans. *Biogeochemistry*, *57*, 47–98. <https://doi.org/10.1023/A:1015798105851>
- Keller, D. P., Oschlies, A., & Eby, M. (2012). A new marine ecosystem model for the University of Victoria Earth System Climate Model. *Geoscientific Model Development*, *5*(5), 1195–1220. <https://doi.org/10.5194/gmd-5-1195-2012>
- Knapp, A. N., Casciotti, K. L., Berelson, W. M., Prokopenko, M. G., & Capone, D. G. (2016). Low rates of nitrogen fixation in eastern tropical South Pacific surface waters. *Proceedings of the National Academy of Sciences*, *113*, 4398–4403. <https://doi.org/10.1073/pnas.1515641113>
- Knapp, A. N., Dekaezemacker, J., Bonnet, S., Sohm, J., & Capone, D. (2012). Sensitivity of Trichodesmium erythraeum and Crocosphaera watsonii abundance and N₂ fixation rates to varying NO₃ and PO₄ concentrations in batch cultures. *Aquatic Microbial Ecology*, *66*(3), 223–236. <https://doi.org/10.3354/ame01577>
- Kustka, A. B., Sa nudo-Wilhelmy, S. A., Carpenter, E. J., Capone, D., Burns, J., & Sunda, W. G. (2003). Iron requirements for dinitrogen- and ammonium-supported growth in cultures of *Trichodesmium* (IMS 101): Comparison with nitrogen fixation rates and iron: Carbon ratios of field populations. *Limnology and Oceanography*, *48*(5), 1869–1884. <https://doi.org/10.4319/lo.2003.48.5.1869>
- Kvale, K., Keller, D. P., Koeve, W., Meissner, K. J., Somes, C., Yao, W., & Oschlies, A. (2020). Explicit silicate cycling in the Kiel Marine Biogeochemistry Model, version 3 (KMBM3) embedded in the Uvic ESCM version 2.9. *Geoscientific Model Development Discussions*, *14*, 7255–7285. <https://doi.org/10.5194/gmd-2020-235>
- Kwiatkowski, L., Yool, A., Allen, J. I., Anderson, T. R., Barciela, R., Buitenhuis, E. T., et al. (2014). iMarNet: An ocean biogeochemistry model intercomparison project within a common physical ocean modelling framework. *Biogeosciences*, *11*(24), 7291–7304. <https://doi.org/10.5194/bg-11-7291-2014>
- Landolfi, A., Dietze, H., Koeve, W., & Oschlies, A. (2013). Overlooked runaway feedback in the marine nitrogen cycle: The vicious cycle. *Biogeosciences*, *10*(3), 1351–1363. <https://doi.org/10.5194/bg-10-1351-2013>
- Landolfi, A., K ahler, P., Koeve, W., & Oschlies, A. (2018). Global marine N₂ fixation estimates: From observations to models. *Frontiers in Microbiology*, *9*, 2112. <https://doi.org/10.3389/fmicb.2018.02112>
- Landolfi, A., Prowe, F. A., Pahlow, M., Somes, C., Chien, C.-T., Schartau, M., et al. (2021). Can top-down controls expand the ecological niche of marine N₂-fixers? *Frontiers in Microbiology*, *12*, 2119. <https://doi.org/10.3389/fmicb.2021.690200>

- Landolfi, A., Somes, C. J., Koeve, W., Zamora, L. M., & Oschlies, A. (2017). Oceanic nitrogen cycling and N₂O flux perturbations in the Anthropocene. *Global Biogeochemical Cycles*, 31(8), 1236–1255. <https://doi.org/10.1002/2017GB005633>
- Laufkötter, C., Vogt, M., Gruber, N., Aita-Noguchi, M., Aumont, O., Bopp, L., et al. (2015). Drivers and uncertainties of future global marine primary production in marine ecosystem models. *Biogeosciences*, 12(23), 6955–6984. <https://doi.org/10.5194/bg-12-6955-2015>
- Luo, C., Mahowald, N., Bond, T., Chuang, P. Y., Artaxo, P., Siefert, R., et al. (2008). Combustion iron distribution and deposition. *Global Biogeochemical Cycles*, 22(1). <https://doi.org/10.1029/2007GB002964>
- Martin, J. H. (1990). Glacial-interglacial CO₂ change: The iron hypothesis. *Paleoceanography*, 5(1), 1–13. <https://doi.org/10.1029/PA005i001p00001>
- Meissner, K. J., Weaver, A. J., Matthews, H. D., & Cox, P. M. (2003). The role of land surface dynamics in glacial inception: A study with the UVic Earth System Model. *Climate Dynamics*, 21(7–8), 515–537. <https://doi.org/10.1007/s00382-003-0352-2>
- Mengis, N., Partanen, A.-I., Jalbert, J., & Matthews, H. D. (2018). 1.5°C carbon budget dependent on carbon cycle uncertainty and future non-CO₂ forcing. *Scientific Reports*, 8(1), 1–7. <https://doi.org/10.1038/s41598-018-24241-1>
- Mills, M. M., Turk-Kubo, K. A., van Dijken, G. L., Henke, B. A., Harding, K., Wilson, S. T., et al. (2020). Unusual marine cyanobacterial/haptophyte symbiosis relies on N₂ fixation even in N-rich environments. *The ISME Journal*, 14(10), 2395–2406. <https://doi.org/10.1038/s41396-020-0691-6>
- Moisander, P. H., Benavides, M., Bonnet, S., Berman-Frank, I., White, A. E., & Riemann, L. (2017). Chasing after non-cyanobacterial nitrogen fixation in marine pelagic environments. *Frontiers in Microbiology*, 8, 1736. <https://doi.org/10.3389/fmicb.2017.01736>
- Moore, C. M., Mills, M. M., Achterberg, E. P., Geider, R. J., LaRoche, J., Lucas, M. I., et al. (2009). Large-scale distribution of Atlantic nitrogen fixation controlled by iron availability. *Nature Geoscience*, 2(12), 867–871. <https://doi.org/10.1038/ngeo667>
- Moore, C. M., Mills, M. M., Arrigo, K. R., Berman-Frank, I., Bopp, L., Boyd, P. W., et al. (2013). Processes and patterns of oceanic nutrient limitation. *Nature Geoscience*, 6(9), 701–710. <https://doi.org/10.1038/ngeo1765>
- Moore, J. K., & Doney, S. C. (2007). Iron availability limits the ocean nitrogen inventory stabilizing feedbacks between marine denitrification and nitrogen fixation. *Global Biogeochemical Cycles*, 21(2). <https://doi.org/10.1029/2006GB002762>
- Mulholland, M. R. (2007). The fate of nitrogen fixed by diazotrophs in the ocean. *Biogeosciences*, 4(1), 37–51. <https://doi.org/10.5194/bg-4-37-2007>
- Nickelsen, L., Keller, D. P., & Oschlies, A. (2015). A dynamic marine iron cycle module coupled to the University of Victoria Earth System Model: The Kiel Marine Biogeochemical Model 2 for UVic 2.9. *Geoscientific Model Development*, 8(5), 1357–1381. <https://doi.org/10.5194/gmd-8-1357-2015>
- Oschlies, A., Koeve, W., Landolfi, A., & Kähler, P. (2019). Loss of fixed nitrogen causes net oxygen gain in a warmer future ocean. *Nature Communications*, 10(1), 1–7. <https://doi.org/10.1038/s41467-019-10813-w>
- Parsons, T. R., Takahashi, M., & Hargrave, B. (1984). *Biological oceanographic processes* (3rd ed.).
- Raven, J. A. (1988). The iron and molybdenum use efficiencies of plant growth with different energy, carbon and nitrogen sources. *New Phytologist*, 109(3), 279–287. <https://doi.org/10.1111/j.1469-8137.1988.tb04196.x>
- Riche, O. G., & Christian, J. R. (2018). Ocean dinitrogen fixation and its potential effects on ocean primary production in Earth system model simulations of anthropogenic warming. *Elementa*, 6. <https://doi.org/10.1525/elementa.277>
- Schlosser, C., Klar, J. K., Wake, B. D., Snow, J. T., Honey, D. J., Woodward, E. M. S., et al. (2014). Seasonal ITCZ migration dynamically controls the location of the (sub)tropical Atlantic biogeochemical divide. *Proceedings of the National Academy of Sciences*, 111(4), 1438–1442. <https://doi.org/10.1073/pnas.1318670111>
- Schmittner, A., Oschlies, A., Matthews, H. D., & Galbraith, E. D. (2008). Future changes in climate, ocean circulation, ecosystems, and biogeochemical cycling simulated for a business-as-usual CO₂ emission scenario until year 4000 AD. *Global Biogeochemical Cycles*, 22(1). <https://doi.org/10.1029/2007GB002953>
- Somes, C. J., & Oschlies, A. (2015). On the influence of “non-Redfield” dissolved organic nutrient dynamics on the spatial distribution of N₂ fixation and the size of the marine fixed nitrogen inventory. *Global Biogeochemical Cycles*, 29(7), 973–993. <https://doi.org/10.1002/2014GB005050>
- Tagliabue, A., Aumont, O., Death, R., Dunne, J. J. P., Dutkiewicz, S., Galbraith, E., et al. (2016). How well do global ocean biogeochemistry models simulate dissolved iron distributions? *Global Biogeochemical Cycles*, 30(2), 149–174. <https://doi.org/10.1002/2015GB005289>
- Tagliabue, A., Barrier, N., Du Pontavice, H., Kwiatkowski, L., Aumont, O., Bopp, L., et al. (2020). An iron cycle cascade governs the response of equatorial Pacific ecosystems to climate change. *Global Change Biology*, 26(11), 6168–6179. <https://doi.org/10.1111/gcb.15316>
- Tagliabue, A., Bowie, A. R., Boyd, P. W., Buck, K. N., Johnson, K. S., & Saito, M. A. (2017). The integral role of iron in ocean biogeochemistry. *Nature*, 543(7643), 51–59. <https://doi.org/10.1038/nature21058>
- Taucher, J., & Oschlies, A. (2011). Can we predict the direction of marine primary production change under global warming? *Geophysical Research Letters*, 38(2). <https://doi.org/10.1029/2010GL045934>
- Tyrrell, T. (1999). The relative influences of nitrogen and phosphorus on oceanic primary production. *Nature*, 400(6744), 525–531. <https://doi.org/10.1038/22941>
- van Vuuren, D. P., Edmonds, J., Kainuma, M., Riahi, K., Thomson, A., Hibbard, K., et al. (2011). The representative concentration pathways: An overview. *Climatic Change*, 109(1–2), 5–31. <https://doi.org/10.1007/s10584-011-0148-z>
- Wang, W.-I., Moore, J. K., Martiny, A. C., & Primeau, F. W. (2019). Convergent estimates of marine nitrogen fixation. *Nature*, 566(7743), 205–211. <https://doi.org/10.1038/s41586-019-0911-2>
- Ward, B. A., Dutkiewicz, S., Moore, C. M., & Follows, M. J. (2013). Iron, phosphorus, and nitrogen supply ratios define the biogeography of nitrogen fixation. *Limnology & Oceanography*, 58(6), 2059–2075. <https://doi.org/10.4319/lo.2013.58.6.2059>
- Weaver, A. J., & Eby, M. (1997). On the numerical implementation of advection schemes for use in conjunction with various mixing parameterizations in the GFDL ocean model. *Journal of Physical Oceanography*, 27(2), 369–377. [https://doi.org/10.1175/1520-0485\(1997\)027<0369:OTNIOA>2.0.CO;2](https://doi.org/10.1175/1520-0485(1997)027<0369:OTNIOA>2.0.CO;2)
- Weaver, A. J., Eby, M., Wiebe, E. C., Bitz, C. M., Duffy, P. B., Ewen, T. L., et al. (2001). The UVic Earth System Climate Model: Model description, climatology, and applications to past, present and future climates. *Atmosphere-Ocean*, 39(4), 361–428. <https://doi.org/10.1080/07055900.2001.9649686>
- Weber, T., & Deutsch, C. (2014). Local versus basin-scale limitation of marine nitrogen fixation. *Proceedings of the National Academy of Sciences of the United States of America*, 111(24), 8741–8746. <https://doi.org/10.1073/pnas.1317193111>
- Wrightson, L., & Tagliabue, A. (2020). Quantifying the impact of climate change on marine diazotrophy: Insights from Earth system models. *Frontiers in Marine Science*, 7, 635. <https://doi.org/10.3389/fmars.2020.00635>
- Yao, W., Kvale, K. F., Achterberg, E., Koeve, W., & Oschlies, A. (2019). Hierarchy of calibrated global models reveals improved distributions and fluxes of biogeochemical tracers in models with explicit representation of iron. *Environmental Research Letters*, 14(11), 114009. <https://doi.org/10.1088/1748-9326/ab4c52>
- Zehr, J. P., & Capone, D. G. (2020). Changing perspectives in marine nitrogen fixation. *Science*, 368(6492), eaay9514. <https://doi.org/10.1126/science.aay9514>